

## A WIDE SYMBIOTIC CHANNEL TO TYPE IA SUPERNOVAE

IZUMI HACHISU

Department of Earth Science and Astronomy, College of Arts and Sciences, University of Tokyo, Komaba,  
Meguro-ku, Tokyo 153-8902, Japan  
e-mail: hachisu@chianti.c.u-tokyo.ac.jp

MARIKO KATO

Department of Astronomy, Keio University, Hiyoshi, Kouhoku-ku, Yokohama 223-8521, Japan  
e-mail: mariko@educ.cc.keio.ac.jp

AND

KEN'ICHI NOMOTO

Department of Astronomy, University of Tokyo, Bunkyo-ku, Tokyo 113-0033, Japan  
e-mail: nomoto@astron.s.u-tokyo.ac.jp  
Research Center for the Early Universe, University of Tokyo, Bunkyo-ku, Tokyo 113-0033, Japan  
*to appear in the Astrophysical Journal, 521, No.2*

### ABSTRACT

As a promising channel to Type Ia supernovae (SNe Ia), we have proposed a symbiotic binary system consisting of a white dwarf (WD) and a low mass red-giant (RG), where strong winds from the accreting WD play a key role to increase the WD mass to the Chandrasekhar mass limit. However, the occurrence frequency of SNe Ia through this channel has been still controversial. Here we propose two new evolutionary processes which make the symbiotic channel to SNe Ia much wider. (1) We first show that the WD + RG close binary can form from a wide binary even with such a large initial separation as  $a_i \lesssim 40000R_\odot$ . Such a binary consists of an AGB star and a low mass main-sequence (MS) star, where the AGB star is undergoing superwind before becoming a WD. If the superwind at the end of AGB evolution is as fast as or slower than the orbital velocity, the wind outflowing from the system takes away the orbital angular momentum effectively. As a result the wide binary shrinks greatly to become a close binary. Then the AGB star undergoes a common envelope (CE) evolution. After the CE evolution, the binary becomes a pair of a carbon-oxygen WD and the MS star. When the MS star evolves to a RG, a WD + RG system is formed. Therefore, the WD + RG binary can form from much wider binaries than our earlier estimate which is constrained by  $a_i \lesssim 1500R_\odot$ . (2) When the RG fills its inner critical Roche lobe, the WD undergoes rapid mass accretion and blows a strong optically thick wind. Our earlier analysis has shown that the mass transfer is stabilized by this wind only when the mass ratio of RG/WD is smaller than 1.15. Our new finding is that the WD wind can strip mass from the RG envelope, which could be efficient enough to stabilize the mass transfer even if the RG/WD mass ratio exceeds 1.15. If this mass-stripping effect is strong enough, though its efficiency is subject to uncertainties, the symbiotic channel can produce SNe Ia for a much (ten times or more) wider range of the binary parameters than our earlier estimation. With the above two new effects (1) and (2), the symbiotic channel can account for the inferred rate of SNe Ia in our Galaxy. The immediate progenitor binaries in this symbiotic channel to SNe Ia may be observed as symbiotic stars, luminous supersoft X-ray sources, or recurrent novae like T CrB or RS Oph, depending on the wind status.

*Subject headings:* binaries: symbiotic — stars: individual (T CrB, RS Oph) — stars: mass-loss — stars: novae — supernovae: general — X-rays: stars

### 1. INTRODUCTION

It is widely accepted that Type Ia supernovae (SNe Ia) are thermonuclear explosions of accreting white dwarfs (e.g., Nomoto, Iwamoto, & Kishimoto 1997). However, whether the explosion of the white dwarf takes at the Chandrasekhar mass limit or at the sub-Chandrasekhar mass has been controversial (e.g., Nomoto et al. 1994; Arnett 1996; Branch 1998). Also the issue of double degenerate (DD) vs. single degenerate (SD) for the progenitor scenario has been still debated (e.g., Branch et al. 1995 for a review).

The DD scenario assumes that merging of double C+O white dwarfs with a combined mass surpassing the Chandrasekhar mass limit induces SN Ia (e.g., Iben & Tutukov 1984; Webbink 1984). However, this scenario has not been well supported. Observationally, the search for DDs has

discovered only several systems whose combined mass is less than the Chandrasekhar mass or whose separation is too wide to merge in a Hubble time (Branch et al. 1995; Renzini 1996; Livio 1996 for reviews). Theoretically, the DD has been suggested to lead to accretion-induced-collapse rather than SN Ia (Nomoto & Iben 1985; Saio & Nomoto 1985, 1998; Segretain et al. 1997).

For the SD scenario, observational counterparts may be symbiotic stars (e.g., Munari & Renzini 1992). Kenyon et al. (1993) and Renzini (1996) have suggested that symbiotics are more likely to lead to the sub-Chandrasekhar mass explosion because the available mass in transfer may not be enough for white dwarfs to reach the Chandrasekhar mass. However, photometric and spectroscopic features of majority of SNe Ia are in much better agreement with the Chandrasekhar mass model than the sub-

Chandrasekhar mass model (Höfllich & Khokhlov 1996; Nugent et al. 1997).

Hachisu, Kato, & Nomoto (1996; hereafter HKN96) have shed new light on the above SD/sub-Chandrasekhar mass scenario and proposed a new progenitor system based on the optically thick wind theory of mass-accreting white dwarfs. In the scenario of Iben & Tutukov (1984) and Webbink (1984), they excluded close binary systems consisting of a mass-accreting white dwarf (WD) and a lobe-filling red(sub)-giant (RG) (first discussed by Whelan & Iben 1973), mainly because such a system suffers from unstable mass transfer when the mass ratio of the RG/WD exceeds 0.79, i.e.,  $q = M_{\text{RG}}/M_{\text{WD}} > 0.79$ . However, HKN96 have shown that optically thick winds from the mass-accreting white dwarf stabilize the mass transfer up to  $q \leq 1.15$  even if the RG has a deep convective envelope. Such an object may be observed as a symbiotic star. Thus they proposed a new channel to SNe Ia, through which a white dwarf accreting mass from a lobe-filling red-giant can grow up to the Chandrasekhar mass limit and explodes as an SN Ia (SD/Chandrasekhar mass scenario of symbiotics).

Li & van den Heuvel (1997) reanalyzed the HKN96 model and identified two isolated regions for SN Ia progenitors in the initial orbital period vs. the initial donor mass plane, i.e., in the  $\log P_0 - M_{\text{d},0}$  plane: 1) One is a relatively compact close binary consisting of a  $M_{\text{d},0} \sim 2 - 3M_{\odot}$  slightly evolved main-sequence companion and a  $M_{\text{WD},0} \sim 1.0 - 1.2M_{\odot}$  white dwarf with the initial orbital periods of  $P_0 \sim 0.5 - 5$  d (hereafter, WD+MS systems), and 2) the other is a relatively wide binary consisting of a low mass ( $M_{\text{d},0} \sim 1M_{\odot}$ ) red-giant companion and a  $M_{\text{WD},0} \sim 1.2M_{\odot}$  white dwarf with the initial orbital periods of  $P_0 \sim 100 - 800$  d (hereafter, WD+RG systems). They also concluded that the new model accounts for the inferred rate of SNe Ia in our Galaxy.

In Li & van den Heuvel's (1997) analysis, their SN Ia progenitor region for the WD+RG system is very small compared with the region for the WD+MS system. The contribution of the WD+RG systems to the total rate of SN Ia explosions was expected to be very small or negligible. It is because the WD+RG channel is restricted by the condition for the stable mass transfer, i.e.,  $q < 1.15$ . In the present paper, we propose a new evolutionary process which makes the WD+RG channel to SN Ia much wider than that of HKN96's original modeling. We include a mass-stripping effect of the red-giant envelope by the wind. The effect removes the limitation of  $q < 1.15$  and, as a result, the new parameter region producing an SN Ia becomes ten times or more wider than the previous region calculated by HKN96 and Li & van den Heuvel (1997).

Recently, Yungelson & Livio (1998) claimed, based on their population synthesis results, that HKN96's and Li & van den Heuvel's (1997) model can account for only, at most, 10% of the inferred rate of SNe Ia. Introducing a new evolutionary process into HKN96's modeling, we have re-analyzed the SN Ia rate for our extended HKN96's model and also for Li & van den Heuvel's model. Our present analysis reveals that the realization frequencies of SNe Ia coming from our WD+RG/WD+MS models are  $\sim 0.002 \text{ yr}^{-1}/\sim 0.001 \text{ yr}^{-1}$ , respectively, and the total SN Ia rate becomes  $\sim 0.003 \text{ yr}^{-1}$ , which is large enough to account for the inferred rate of SN Ia rate in our Galaxy. There are

three reasons why our estimates are much larger than Yungelson & Livio's (1998) estimates: 1) We introduce a mass-stripping process into the WD+RG systems as an extension of HKN96's model. As a result, the new parameter region producing an SN Ia becomes ten times or more wider than the previous region calculated by HKN96 and Li & van den Heuvel (1997) when the efficiency of the mass-stripping effect is strong enough. 2) Yungelson & Livio (1998) assumed that the initial separation is *smaller than*  $a_i \lesssim 1500 R_{\odot}$  in their estimations of the WD+RG model. If one includes the effect of angular momentum loss by slow winds at the end of stellar evolution, however, very wide binaries with the separation of  $1500 R_{\odot} \lesssim a_i \lesssim 40000 R_{\odot}$  shrink into  $30 R_{\odot} \lesssim a_f \lesssim 800 R_{\odot}$ , which provide appropriate initial conditions for our WD+RG models. 3) We believe that Yungelson & Livio (1998) did not include an important evolutionary path in the rate estimation for Li & van den Heuvel's (1997) WD+MS model. They assumed that relatively massive white dwarfs ( $\sim 1M_{\odot}$ ) are born from an AGB star and neglected the possibility that it comes from a helium star whose hydrogen-rich envelope is stripped away in a common envelope evolution at the red-giant phase with a helium core. Very recently, including the evolutionary path mentioned above, Hachisu, Kato, Nomoto, & Umeda (1999, hereafter HKNU99) have shown that the realization frequency for the WD+MS systems is as large as  $\nu_{\text{MS}} \sim 0.001 \text{ yr}^{-1}$ , which accounts for one third of the inferred rate of SNe Ia in our Galaxy.

It has been argued that some of the recurrent novae are progenitors of SNe Ia (e.g., Starrfield et al. 1988) because these white dwarfs are suggested to be very massive and close to the Chandrasekhar mass limit. Morphologically, recurrent novae are divided into three groups according to the companion star; dwarf companions, slightly evolved main-sequence (or sub-giant) companions, and red-giant companions (Schaefer & Ringwald 1995). The latter two groups are relevant to SNe Ia progenitors and the good examples are as follows.

1) T CrB ( $P_{\text{orb}} = 227.67$  d; e.g., Lines et al. 1988) and RS Oph ( $P_{\text{orb}} = 460$  d; Dobrzycka & Kenyon 1994) belong to the last group of red-giant companions and their white dwarf masses are very close to the Chandrasekhar mass limit (e.g., Kato 1990, 1995, 1999; Shahbaz et al. 1997; Belczyński & Mikolajewska 1998; Hachisu & Kato 1999a). These two systems correspond to the WD+RG systems. These extremely massive white dwarfs are naturally explained in our SN Ia progenitor scenario.

2) On the other hand, U Sco ( $P_{\text{orb}} = 1.23$  d; Schaefer & Ringwald 1995) and V394 CrA ( $P_{\text{orb}} = 0.758$  d; Schaefer 1990) belong to the middle group of the slightly evolved main-sequence companions. For this group, it has been suggested that the companion has an extremely helium-rich envelopes and the primary is a very massive white dwarfs close to the Chandrasekhar mass limit. Our WD+MS model yields the secondary star having a helium-rich envelope as well as the primary of very massive white dwarfs as suggested first by Hachisu & Kato (1999b).

In §2, we describe a new idea of mass-stripping effect by strong winds and the mass accumulation efficiency. We then search for the initial parameter regions that can produce SNe Ia in §3. In §4, we discuss relevance to recurrent novae, our criticism to Yungelson & Livio's claims, esti-

mation of SN Ia rates of the WD+RG/WD+MS systems, and the possibility of detecting hydrogen-lines at SN Ia explosions during the strong wind phase. Conclusions follow in §5.

## 2. PROGENITOR SYSTEMS

First of all, we illustrate a full evolutionary path of our WD+RG system from the zero age main-sequence stage (*stage A*) to the SN Ia explosion (*stage F*) in Figure A1.

- A) Zero age main-sequence.
- B) The primary has evolved first to become an AGB star and blows a slow wind (or a super wind) at the end of stellar evolution.
- C) The slow wind carries the orbital angular momentum and, as a reaction, the separation shrinks considerably (by about a factor of ten or more), which is a similar process to the common envelope evolution.
- D) A carbon-oxygen white dwarf (the initial primary) and a zero age main-sequence star (the initial secondary) remain.
- E) The initial secondary has evolved to a red-giant forming a helium core and fills up its inner critical Roche lobe. Mass transfer begins. The WD component blows a strong wind and the winds can stabilize the mass transfer even if the RG component has a deep convective envelope.
- F) The WD component has grown in mass to the Chandrasekhar mass limit and explodes as a Type Ia supernova.

For an immediate progenitor system of Type Ia supernovae (SNe Ia), we consider a close binary initially consisting of a carbon-oxygen white dwarf (C+O WD) with  $M_{\text{WD},0} = 0.6 - 1.2M_{\odot}$  and a low-mass red-giant star with  $M_{\text{RG},0} = 0.7 - 3.0M_{\odot}$  having a helium core of  $M_{\text{He},0} = 0.2 - 0.46M_{\odot}$  (*stage E*). The initial state of these immediate progenitors is specified by three parameters, i.e.,  $M_{\text{WD},0}$ ,  $M_{\text{RG},0}$ , and the initial orbital period  $P_0$  ( $M_{\text{He},0}$  is determined if  $P_0$  is given). We follow binary evolutions of these systems by using empirical formulae (Webbink et al. 1983) and obtain the parameter range(s) which can produce an SN Ia.

### 2.1. Conventional evolution scheme

When the companion evolves to a red-giant (RG) and fills its inner critical Roche lobe, mass transfer begins from the RG to the WD. If both the total mass and the total angular momentum are conserved and the mass transfer is steady, its rate is given by

$$\frac{\dot{M}_2}{M_2} = \left( \frac{\dot{R}_2}{R_2} \right)_{\text{EV}} / H(q), \quad (1)$$

where  $(\dot{R}_2/R_2)_{\text{EV}}$  represents specifically the evolutionary change in the secondary radius and

$$H(q) = \frac{d \ln f(q)}{d \ln q} (1+q) - 2(1-q), \quad (2)$$

where  $q$  is the mass ratio defined by

$$q \equiv M_2/M_1, \quad (3)$$

( $M_1$  is the mass of the primary, i.e., the WD component, and  $M_2$  the mass of the secondary, i.e., the RG component). Here we use the empirical formula proposed by Eggleton (1983),

$$\frac{R_2^*}{a} = f(q) = \frac{0.49q^{2/3}}{0.6q^{2/3} + \ln(1+q^{1/3})}, \quad (4)$$

for an effective radius ( $R_2^*$ ) of the secondary's inner critical Roche lobe. For the separation  $a$ , we simply assume a circular orbit. To estimate  $(\dot{R}_2/R_2)_{\text{EV}}$  we use the empirical formulae proposed by Webbink et al. (1983).

For a sufficiently large mass of the secondary  $M_2$  (i.e.,  $q > 0.79$ ), however, equation (1) gives a positive value of  $\dot{M}_2$ . This means that the mass transfer proceeds not on an evolutionary time scale but rather on a thermal or dynamical time scale. The gas falls very rapidly onto the WD and forms an extended envelope around the WD (e.g., Nomoto et al. 1979; Iben 1988). This envelope expands to fill the inner and then outer critical Roche lobe. It eventually results in the formation of a common envelope, in which the two cores are spiraling in each other. It forms a very compact binary system consisting of a C+O WD and a helium WD, or a merger of C+O and He cores. These systems have been extensively examined by many authors (e.g., Iben & Livio 1993 for a review and references therein).

### 2.2. White Dwarf Winds

However, the recent version of opacity (Iglesias & Rogers 1996) has changed the story. Optically thick winds are driven when the WD envelope expands and the photospheric temperature decreases below  $\log T_{\text{ph}} \sim 5.5$  (Kato & Hachisu 1994). We have calculated such wind solutions for various white dwarf masses of  $M_{\text{WD}} = 0.6, 0.7, 0.8, 0.9, 1.0, 1.1, 1.2, 1.3, 1.35$  and  $1.377M_{\odot}$  and show six of ten cases, i.e.,  $M_{\text{WD}} = 0.6, 0.8, 1.0, 1.2, 1.3$  and  $1.377M_{\odot}$  in Figures A2–A6. Here, we choose  $1.377M_{\odot}$  as a limiting mass just below the mass at the SN Ia explosion in W7 ( $1.378M_{\odot}$ , Nomoto et al. 1984) as was done in Kato (1995, 1999). We have used the updated OPAL opacity (Iglesias & Rogers 1996) because its strong peak near  $\log T \sim 5.2$  is about 20–30% larger than that of the original OPAL opacity (Rogers & Iglesias 1992) which was used in HKN96. The numerical method and various assumptions are the same as in Kato & Hachisu (1994) so that we omit the details of the numerical calculations to avoid the duplication. The only difference between the results in HKN96 (or Kato & Hachisu 1994) and the present ones is the opacity as mentioned above.

Each wind solution is a unique function of the envelope mass  $\Delta M$  if the white dwarf mass is given. The envelope mass is decreasing due to wind mass loss  $\dot{M}_{\text{wind}} (< 0)$  and hydrogen shell burning  $\dot{M}_{\text{nuc}} (< 0)$ , i.e.,

$$\frac{d}{dt} \Delta M = -\dot{M}_2 + \dot{M}_{\text{wind}} + \dot{M}_{\text{nuc}}. \quad (5)$$

When the mass transfer rate from the companion  $\dot{M}_2 (< 0)$  does not vary so much in a thermal time scale of the WD envelope, the WD envelope reaches an equilibrium of

$$\dot{M}_2 = \dot{M}_{\text{wind}} + \dot{M}_{\text{nuc}}. \quad (6)$$

Thus we regard the ordinates in Figures A2–A6 as the mass transfer rate from the companion.

Figure A2 shows the envelope mass of the wind and static solutions against the total mass decreasing rate of the envelope  $|dM/dt|$ , i.e., the mass transfer rate from the companion  $|\dot{M}_2|$ . There exists only a static (no wind) solution below the break of each solid line while there exists only a wind solution above the break for a given envelope mass of  $\Delta M$ . The optically thick winds blow when the mass transfer rate from the companion star  $|\dot{M}_2| = |\dot{M}_{\text{nuc}} + \dot{M}_{\text{wind}}|$  exceeds

$$\dot{M}_{\text{cr}} \approx 0.75 \times 10^{-6} \left( \frac{M_{\text{WD}}}{M_{\odot}} - 0.40 \right) M_{\odot} \text{ yr}^{-1}, \quad (7)$$

which is reduced from our wind/static solutions as shown in Figure A2. Figure A3 shows the photospheric temperature against the mass transfer rate. It should be noted that the optically thick winds begin near  $\log T \sim 5.5$ , which corresponds to the shoulder of the strong peak of OPAL opacity in the high temperature side. Figure A4 depicts the photospheric radius against the mass transfer rate. The optically thick winds occur when the photosphere expands to  $R_{\text{ph}} \sim 0.1 R_{\odot}$ , which is much smaller than the inner critical Roche lobe. We plot the photospheric velocity  $v_{\text{ph}}$  in Figure A5 and the ratio  $v_{\text{ph}}/v_{\text{esc}}$  between the photospheric velocity and the escape velocity at the photosphere in Figure A6 against the mass transfer rate. Here, we call the wind as “strong” when the photospheric velocity exceeds the escape velocity there. When the wind is strong enough, the photospheric velocity is as high as  $\sim 1000 \text{ km s}^{-1}$  being much faster than the orbital velocity, i.e.,  $v_{\text{ph}} \gg a\Omega_{\text{orb}}$ .

The optically thick wind is a continuum-radiation driven wind in which the acceleration occurs deep inside the photosphere (e.g., Kato & Hachisu 1994). Further acceleration of the wind near the photosphere is negligibly small because the photon momentum near the photosphere is much smaller than the momentum of the wind. Therefore, our results are almost independent of the treatment of the radiative transfer near the photosphere. In other words, the critical points of the wind solutions, where the wind is accelerated, exist deep inside the photosphere and also deep inside the inner critical Roche lobe for our WD+RG systems. This means that the binary motion does not affect the acceleration of the optically thick winds mainly because the strong winds are already accelerated deep inside the inner critical Roche lobe up to the velocity much faster than the orbital motion.

Once the strong wind occurs, the mass transfer rate is modified as

$$\frac{\dot{M}_2}{M_2} = \left( \left( \frac{\dot{R}_2}{R_2} \right)_{\text{EV}} - H_1(q) \left( \frac{\dot{M}_1}{M_1} \right) \right) / H_2(q), \quad (8)$$

$$H_1(q) = -\frac{d \ln f(q)}{d \ln q} + \frac{1}{1+q} - 2 + 2\ell_w \frac{1+q}{q}, \quad (9)$$

$$H_2(q) = \frac{d \ln f(q)}{d \ln q} + \frac{q}{1+q} - 2 + 2\ell_w(1+q), \quad (10)$$

where  $\ell_w$  is the specific angular momentum of the wind in units of  $a^2\Omega_{\text{orb}}$ ,

$$\left( \frac{j}{M} \right)_{\text{wind}} = \ell_w a^2 \Omega_{\text{orb}}, \quad (11)$$

$J$  the total angular momentum,  $M$  the total mass of the system, and  $\Omega_{\text{orb}}$  the orbital angular velocity. The wind velocity is about several hundred to one thousand  $\text{km s}^{-1}$  for relatively massive WDs when the mass transfer rate is  $\lesssim 1 \times 10^{-5} M_{\odot} \text{ yr}^{-1}$  (Fig. A5). The wind velocity is about ten times faster than the orbital velocity because of  $a\Omega_{\text{orb}} \sim 30 - 100 \text{ km s}^{-1}$  for  $M_{\text{WD}} \sim 1 M_{\odot}$ ,  $M_2 \sim 1 M_{\odot}$ , and  $a \sim 30 - 400 R_{\odot}$ . In such cases, winds cannot get angular momentum from the orbital motion by torque during its journey, so that wind has the same specific angular momentum as the WD, which is estimated as

$$\ell_w = \left( \frac{q}{1+q} \right)^2. \quad (12)$$

In this case, function  $H_2(q)$  changes its sign at  $q = 1.15$ . Wind mass loss stabilizes the mass transfer in the region from  $q = 0.79$  to  $q = 1.15$  (HKN96).

### 2.3. Growth of white dwarfs

During the strong wind phase, as hydrogen steadily burns on the surface of the WD, the WD accretes the processed matter approximately at a rate of  $\dot{M}_{\text{cr}}$ , which is given in equation (7). When the mass transfer rate decreases below this critical value, optically thick winds stop. If the mass transfer rate further decreases below

$$\dot{M}_{\text{st}} \approx \frac{1}{2} \dot{M}_{\text{cr}}, \quad (13)$$

which is also reduced from our solutions for the minimum envelope mass corresponding to the lower end of each solid lines in Figure A2, hydrogen shell burning becomes unstable to trigger very weak shell flashes. Once a shell flash occurs, a part of the transferred hydrogen-rich matter may be blown off and we need to estimate the net mass accumulation in order to examine whether or not the WD will grow up to the Chandrasekhar mass limit (e.g., Kovetz & Prialnik 1994). Here, we roughly assume that all the processed matter is retained until the accretion rate becomes below

$$\dot{M}_{\text{low}} = \frac{1}{8} \dot{M}_{\text{cr}} \sim 1 \times 10^{-7} M_{\odot} \text{ yr}^{-1}. \quad (14)$$

This assumption may slightly underestimate the mass loss from the WD, but there still exists a large uncertainty in relation to the mass accumulation ratio,  $\eta_{\text{H}}$ , i.e., the ratio of the retained mass to the transferred mass after many cycles of hydrogen shell flashes. To summarize, we assume the mass accumulation ratio of hydrogen shell burning as

$$\eta_{\text{H}} = \begin{cases} 0, & \text{for } |\dot{M}_2| \leq \dot{M}_{\text{low}} \\ 1, & \text{for } \dot{M}_{\text{low}} < |\dot{M}_2| < \dot{M}_{\text{cr}} \\ 1 - \dot{M}_w / \dot{M}_2, & \text{for } \dot{M}_{\text{cr}} \leq |\dot{M}_2| \lesssim \dot{M}_{\text{high}} \end{cases} \quad (15)$$

where  $\dot{M}_w$  is the wind mass loss rate calculated by the optically thick wind theory and  $\dot{M}_{\text{high}} \sim 1 \times 10^{-4} - 1 \times 10^{-3} M_\odot \text{ yr}^{-1}$  is the upper limit of the mass transfer rate for our wind solutions as shown in Figure A2.

The steady hydrogen shell burning converts hydrogen into helium atop the C+O core and increases the mass of the helium layer gradually. When its mass reaches a certain value, helium ignites. For the accretion rate given by equation (7), helium shell burning is unstable to grow to a weak flash. Once a helium shell flash occurs on relatively massive white dwarfs ( $M_{\text{WD}} \gtrsim 1.2 M_\odot$ ), a part of the envelope mass is blown off in the wind (Kato et al. 1989). Recently, Kato & Hachisu (1999) have recalculated the mass accumulation efficiency for helium shell flashes with the new opacity (Iglesias & Rogers 1996). Here, we adopt their new results in a simple analytic form,

$$\eta_{\text{He}} = \begin{cases} -0.175 \left( \log \dot{M}_{\text{He}} + 5.35 \right)^2 + 1.05, & \text{for } -7.3 < \log \dot{M}_{\text{He}} < -5.9 \\ 1, & \text{for } -5.9 \leq \log \dot{M}_{\text{He}} \lesssim -5 \end{cases} \quad (16)$$

where the mass accretion rate,  $\dot{M}_{\text{He}}$ , is in units of  $M_\odot \text{ yr}^{-1}$  and given by

$$\dot{M}_{\text{He}} = \eta_{\text{H}} \cdot |\dot{M}_2|, \quad (17)$$

when hydrogen-rich matter is transferred from the companion star. Eventually, we have the growth rate of C+O WDs given by

$$\dot{M}_{\text{C+O}} = \eta_{\text{He}} \cdot \dot{M}_{\text{He}} = \eta_{\text{He}} \cdot \eta_{\text{H}} \cdot |\dot{M}_2|, \quad (18)$$

in our WD+RG systems. We use formula (16) for various white dwarf masses and accretion rates, although their results are given only for a  $1.3 M_\odot$  white dwarf (Kato & Hachisu 1999).

The wind velocity in helium shell flashes reaches as high as  $\sim 1000 \text{ km s}^{-1}$ , which is much faster than the orbital velocities of our WD+MS binary systems, i.e.,  $a\Omega_{\text{orb}} \sim 300 \text{ km s}^{-1}$  or of our WD+RG binary systems, i.e.,  $a\Omega_{\text{orb}} \sim 30 \text{ km s}^{-1}$ . It should be noted here that either a Roche lobe overflow or a common envelope does not play a role as a mass ejection mechanism because the envelope matter goes away quickly from the system without interacting with the orbital motion (see Kato & Hachisu 1999 for more details).

#### 2.4. Mass-stripping effect

We propose here a new effect, namely, stripping of a red-giant envelope by the wind, which is not included in HKN96's modeling. Very fast strong winds collide with the surface of the companion as illustrated in Figure A1 (*stage E*) and, for more detail, in Figure A7. The red-giant surface is shock-heated and ablated in the wind. We estimate the shock-heating by assuming that the velocity component normal to the red-giant surface is dissipated by shock and its kinetic energy is converted into the thermal energy of the surface layer of the red-giant envelope (see Fig. A7). The very surface layer of the envelope expands to be easily ablated in the wind. To obtain the mass stripping rate, we equate the rate times the gravitational potential at the red-giant surface to the net dissipation energy per unit time by the shock, i.e.,

$$-\frac{GM_2}{R_2} \left( d\dot{M}_2 \right)_{\text{strip}} = \eta_{\text{eff}} \cdot \frac{1}{2} v^2 \sin^2 \beta \cdot \rho v \sin \beta$$

$$\times 2\pi R_2^2 \sin \theta d\theta, \quad (19)$$

between  $\theta$  and  $\theta + d\theta$ , where

$$\alpha + \beta + \theta = \frac{\pi}{2}, \quad (20)$$

$$\frac{R_2}{\sin \alpha} = \frac{a}{\sin(\pi/2 + \beta)}, \quad (21)$$

$$\begin{aligned} \theta &= \cos^{-1} \left( \frac{R_2}{a} \cos \beta \right) - \beta \\ &= \cos^{-1} (f(q) \cdot \cos \beta) - \beta, \end{aligned} \quad (22)$$

under the condition of  $\beta \geq 0$  (See Fig. A7). Here  $v$  is the wind velocity,  $R_2/a$  is replaced with  $f(q)$  given in equation(4), and  $\eta_{\text{eff}}$  is a numerical factor representing the efficiency of the energy which is transferred to ablation. We assume  $\eta_{\text{eff}} = 1$  in the present calculation but examine the case of  $\eta_{\text{eff}} = 0.3$  for comparison. By integrating over  $\theta$  and using the wind mass loss rate  $\dot{M}_w$  (negative) given by

$$\dot{M}_w = -4\pi r^2 \rho v, \quad (23)$$

we have

$$\frac{GM_2}{R_2} \cdot \left( \dot{M}_2 \right)_{\text{strip}} = \frac{1}{2} v^2 \dot{M}_w \cdot \eta_{\text{eff}} \cdot g(q). \quad (24)$$

Here  $g(q)$  is the geometrical factor of the red-giant surface hit by the wind including dissipation effect (Fig. A7) and it is only a function of the mass ratio  $q$ . Then, the stripping rate of the red-giant envelope is estimated as

$$\dot{M}_s \equiv \left( \dot{M}_2 \right)_{\text{strip}} = \eta_{\text{eff}} \cdot \frac{v^2 R_2}{2GM_2} \dot{M}_w \cdot g(q), \quad (25)$$

$$g(q) = \int_{\beta=\pi/2}^{\beta=0} \frac{1}{2} \sin^3 \beta \frac{R_2^2}{r^2} \sin \theta d\theta, \quad (26)$$

where some numerical values of  $g(q)$  are given in Table A1. The total angular momentum loss rate by stripping is also estimated as

$$\left( \dot{J} \right)_{\text{strip}} = \eta_{\text{eff}} \cdot \frac{v^2 R_2}{2GM_2} \dot{M}_w a^2 \Omega_{\text{orb}} \cdot h(q), \quad (27)$$

$$\begin{aligned} h(q) &= \int_{\beta=\pi/2}^{\beta=0} \frac{1}{2} \sin^3 \beta \frac{R_2^2}{r^2} \sin \theta d\theta \\ &\times \left( \frac{1}{1+q} - \frac{R_2}{a} \cos \theta \right)^2, \end{aligned} \quad (28)$$

$$\left( \frac{\dot{J}}{\dot{M}} \right)_{\text{strip}} = \ell_s a^2 \Omega_{\text{orb}} = \frac{h(q)}{g(q)} \cdot a^2 \Omega_{\text{orb}}, \quad (29)$$

where the ablated gas is assumed to have the angular momentum at the red-giant surface. We note that the numerical factor  $\ell_s = h(q)/g(q)$  given in Table A1 is rather small compared with  $\ell_w$  in equation (12).

Including the effect of mass-stripping, we estimate the mass transfer rate from the secondary to the primary ( $\dot{M}_t < 0$ ) as

$$\frac{\dot{M}_t}{M_2} = \left( \left( \frac{\dot{R}_2}{R_2} \right)_{\text{EV}} - H_3(q) \left( \frac{\dot{M}_{\text{cr}}}{M_1} \right) \right) / H_4(q), \quad (30)$$

$$H_3(q) = H_1(q) + \frac{c_1}{q} H_2(q) + 2(\ell_s - \ell_w)(1+q) \frac{c_1}{q}, \quad (31)$$

$$H_4(q) = (1 + c_1)H_2(q) + 2(\ell_s - \ell_w)(1+q)c_1, \quad (32)$$

$$c_1 \equiv \eta_{\text{eff}} \cdot \frac{v^2 R_2}{2GM_2} \cdot g(q), \quad (33)$$

where  $c_1$  is a numerical factor indicating stripping effect as

$$\dot{M}_s = c_1 \dot{M}_w, \quad (34)$$

and estimated as

$$c_1 \sim \eta_{\text{eff}} \left( \frac{g(q)}{0.025} \right) \left( \frac{v}{1000 \text{ km s}^{-1}} \right)^2 \times \left( \frac{R_2}{30R_\odot} \right) \left( \frac{M_2}{2M_\odot} \right)^{-1}. \quad (35)$$

The stripping effect is important, i.e.,  $c_1 \sim 1$ , when the orbital period is longer than  $P \sim 30$  d for  $\eta_{\text{eff}} = 1$ ,  $M_{\text{WD}} = 1.0M_\odot$ ,  $M_2 = 2.0M_\odot$ , and  $v = 1000 \text{ km s}^{-1}$ . Function  $H_4(q)$  remains negative even for  $q > 1.15$  because the second term in the right hand side of equation (32) is always negative, i.e.,  $\ell_s < \ell_w$ . Therefore, the mass stripping effect stabilizes the mass transfer even for  $q > 1.15$ , so that the limitation of  $q < 1.15$  proposed by HKN96 for stable mass transfer is removed.

### 3. RESULTS

Our progenitor system can be specified by three initial parameters: the WD mass  $M_{\text{WD},0}$ , the red-giant mass  $M_{\text{RG},0}$ , and the orbital period  $P_0$ . We study three cases P1-P3 (P stands for Progenitor) of such close binary evolutions. We start the calculation when the secondary fills its inner critical Roche lobe. The initial parameters ( $M_{\text{WD},0}$ ,  $M_{\text{RG},0}$ ,  $P_0$ ) are summarized in Table A2. For example,  $M_{\text{WD},0} = 1.0M_\odot$ ,  $M_{\text{RG},0} = 2.0M_\odot$ , and  $P_0 = 300$  d for case P1. The evolutionary histories are plotted in Figures A8-A10. In these three cases, the WDs grow up to  $M_{\text{Ia}} = 1.38M_\odot$  to trigger an SN Ia explosion as follows.

- P1) The mass transfer begins at a rate of  $\dot{M}_t = -8.7 \times 10^{-7} M_\odot \text{ yr}^{-1}$ , and then the WD wind starts to blow at a mass loss rate of  $\dot{M}_w = -4.8 \times 10^{-7} M_\odot \text{ yr}^{-1}$ ; and the wind then induces the mass stripping at a rate of  $\dot{M}_s = -2.0 \times 10^{-6} M_\odot \text{ yr}^{-1}$ . Thus a half of the transferred matter is blown off in the wind. The mass transfer rate gradually decreases because of decreasing  $M_2/M_{\text{WD}}$  but still higher than  $\dot{M}_{\text{cr}}$  just when the WD mass reaches  $M_{\text{Ia}}$  and explodes as an SN Ia at  $t = 7.2 \times 10^5$  yr during the WIND phase (Fig. A8).
- P2) The mass transfer, the WD wind, and the mass stripping start as in case P1 at a rate of  $\dot{M}_t$ ,  $\dot{M}_w$ , and

$\dot{M}_s$  as summarized in Table A2. Thus two thirds of the transferred matter accumulates onto the WD. The mass transfer rate is gradually decreasing and becomes lower than  $\dot{M}_{\text{cr}}$  at  $t = 6.7 \times 10^5$  yr. The wind stops but nuclear burning is still stable until the WD mass reaches  $M_{\text{Ia}}$  to explode as an SN Ia at  $t = 7.4 \times 10^5$  yr (Fig. A9). After the wind stops, the progenitor may be observed as a luminous super-soft X-ray source (SSS).

- P3) The mass transfer, the WD wind, and the mass stripping start at the rate summarized in Table A2. In this case, a large part of the transferred matter is accumulating onto the WD. The mass transfer rate decreases and becomes lower than  $\dot{M}_{\text{cr}}$  at  $t = 5.3 \times 10^5$  yr. The wind stops but the nuclear burning is still stable until  $t = 6.5 \times 10^5$  yr. The progenitor may be observed as an SSS during this steady hydrogen shell burning phase. Then nuclear burning becomes unstable to trigger very weak shell flashes but most of the processed matter accumulates onto the WD. The progenitor may be observed as a recurrent nova (RN). The WD mass eventually reaches  $M_{\text{Ia}}$  to explode as an SN Ia at  $t = 1.04 \times 10^6$  yr (Fig. A10).

We have three cases of the immediate progenitors of our WD+RG systems corresponding to cases P1-P3, which are summarized in Table A3, i.e., P1) wind phase (denoted by WIND), P2) steady nuclear burning phase (denoted by SSS), and P3) unsteady weak shell flash phase (denoted by RN). In cases P2 and P3, the SSS phase is rather short compared with the wind phase. Therefore, the frequencies of the SSS phase may be small in our symbiotic channel to SNe Ia.

The final outcome of the binary evolution is summarized in the  $\log P_0 - M_{\text{d},0}$  plane (Fig. A11). The right region of long  $P_0$  in the figure represents our new results of the WD+RG system. In the left region of short  $P_0$ , we also show the results of the WD+MS system for comparison (see HKNU99 for details). Each grid in the  $\log P_0 - M_{\text{d},0}$  plane corresponds to the evolutionary model of our wide WD+RG systems (labeled by ‘‘WD+RG system’’) together with the compact WD+MS systems (labeled by ‘‘WD+MS system’’; HKNU99). Here,  $M_{\text{d},0}$  is the mass of the donor, i.e.,  $M_{\text{RG},0}$  (the initial mass of the red-giant component), or  $M_{\text{MS},0}$  (the initial mass of the slightly evolved main-sequence component). The initial mass of the white dwarf is assumed to be  $M_{\text{WD},0} = 1.0M_\odot$ .

The outcome of the evolution at the end of our calculations is classified as follows.

- i) Formation of a common envelope where the mass transfer is unstable ( $H_4(q) > 0$ ) at the beginning of mass transfer (denoted by  $\times$ ).
- ii) SN Ia explosions (denoted by  $\oplus$  corresponding to case P1,  $\circ$  corresponding to case P2, and  $\odot$  corresponding to case P3), where the WD mass reaches  $1.38 M_\odot$ .
- iii) Novae or strong hydrogen shell flash (denoted by open triangle), where the mass transfer rate becomes below  $\dot{M}_{\text{low}}$ .

- iv) Helium core flash of the red giant component (denoted by filled triangle) where a central helium core flash ignites, i.e., the helium core mass of the red-giant reaches  $0.46M_{\odot}$ .

The region enclosed by the thin solid line produces SNe Ia. In HKN96's model, this region was limited by  $M_{\text{RG},0} < 1.15M_{\odot}$  for  $M_{\text{WD},0} = 1M_{\odot}$ . This new area is about ten times or more wider than that of HKN96's modeling.

We also show, in Figure A12, other three cases of the initial WD mass,  $M_{\text{WD},0} = 0.8M_{\odot}$ ,  $0.9M_{\odot}$ , and  $1.1M_{\odot}$  (thin solid) together with  $M_{\text{WD},0} = 1.0M_{\odot}$  (thick solid). The regions of  $M_{\text{WD},0} = 0.6M_{\odot}$  and  $0.7M_{\odot}$  vanish for both the WD+MS and WD+RG systems. It is clear that the new region of the WD+RG system is not limited by the condition of  $q < 1.15$ , thus being ten times or more wider than the region of HKN96's model for the other initial white dwarf masses.

For  $M_{\text{WD},0} > 1.2M_{\odot}$ , the central density of the WD reaches  $\sim 10^{10} \text{ g cm}^{-3}$  before heating wave from the hydrogen burning layer reaches the center. As a result, the WD undergoes collapse due to electron capture without exploding as an SN Ia (Nomoto & Kondo 1991).

To examine the effect of the stripping parameter,  $\eta_{\text{eff}}$ , we show, in Figure A13, the regions of SN Ia explosion for  $\eta_{\text{eff}} = 0.3$ . Here, four cases of  $M_{\text{WD},0} = 0.9, 1.0, 1.1,$  and  $1.2M_{\odot}$  are depicted. The region of  $M_{\text{WD},0} = 1.0M_{\odot}$  for  $\eta_{\text{eff}} = 0.3$  is one third, in area, of the region for  $\eta_{\text{eff}} = 1$  (see the region enclosed by the dash-dotted line in Fig. A12). In the limiting case of  $\eta_{\text{eff}} = 0$ , we have again the constraint of  $q < 1.15$  as in HKN96's modeling.

#### 4. DISCUSSION

##### 4.1. Recurrent novae as progenitors of SNe Ia

First, we introduce a few binary systems which are well understood in relation to our SN Ia progenitor model. T Coronae Borealis (T CrB) and RS Ophiuchi (RS Oph) are recurrent novae, which are binaries consisting of a very massive white dwarf and a lobe-filling red-giant with orbital periods of 228 d (Lines et al. 1988) and 460 d (Dobrzycka & Kenyon 1994), respectively. Two interpretations have been proposed so far on the binary nature of T CrB: one is an episodic mass transfer event (model) onto a main-sequence star from a red-giant companion (e.g. Webbink et al. 1987) and the other is a thermonuclear runaway event (model) on a mass-accreting white dwarf as massive as the Chandrasekhar mass limit (e.g., Selvelli et al. 1992). Ultra-violet lines in its quiescent phase observed by *IUE* strongly indicate the existence of a mass-accreting white dwarf instead of a main-sequence star (Selvelli et al. 1992).

Very rapid decline rates of their light curves indicate a very massive white dwarf close to the Chandrasekhar limit, that is,  $M_{\text{WD}} \sim 1.37 - 1.38M_{\odot}$  for T CrB (Kato 1995, 1999). It should be noted that Kato (1995, 1999) calculated the nova light curves for the white dwarf masses of 1.2, 1.3, 1.35 and  $1.377M_{\odot}$ , where  $1.377M_{\odot}$  was chosen as a limiting mass being just below the mass at the SN Ia explosion in the W7 model ( $1.378M_{\odot}$ , Nomoto et al. 1984). Kato found that the light curve of the  $1.377M_{\odot}$  model is in better agreement with observational light curve of T CrB than the lower mass models.

Very recently, other observational supports for a massive white dwarf in T CrB have been reported: one is

$M_{\text{WD}} = 1.2 \pm 0.2M_{\odot}$  by Belczyński and Mikolajewska (1998) and the other is  $M_{\text{WD}} = 1.3 - 2.5M_{\odot}$  by Shahbaz et al. (1997). Belczyński and Mikolajewska derived a permitted range of binary parameters from amplitude of the ellipsoidal variability and constraints from the orbital solution of M-giants. The white dwarf mass is permitted up to  $1.44M_{\odot}$  under the condition of a certain mass ratio and inclination of the orbit (in their Fig. 4). In Shahbaz et al. (1997), a massive white dwarf of  $M_{\text{WD}} = 1.3 - 2.5M_{\odot}$  in T CrB is also suggested from the infrared light curve fitting. Combining these two permitted ranges of the white dwarf mass in T CrB, we may conclude that a mass of the white dwarf is between  $M_{\text{WD}} = 1.3 - 1.4M_{\odot}$ , which is very consistent with the light curve analysis ( $M_{\text{WD}} \sim 1.37 - 1.38M_{\odot}$  of T CrB) by Kato (1999).

However, it is very unlikely that such very massive white dwarfs were born at the end of single star evolution in a binary (e.g., Weidemann 1986; see also eq.(2) of Yungelson et al. 1993). It is more likely that a less massive white dwarf accretes hydrogen-rich matter from a red-giant companion and grows up to near the Chandrasekhar limit. If we include the mass-stripping effect by the strong WD wind, we easily reproduce the present states of T CrB and RS Oph systems.

Specifying the initial parameters of  $M_{\text{WD},0} = 1.0M_{\odot}$ ,  $M_{\text{RG},0} = 1.3M_{\odot}$ , and  $P_0 = 135$  d, we obtain the present state of  $M_{\text{WD}} = 1.37M_{\odot}$ ,  $M_{\text{RG}} = 0.71M_{\odot}$  (with a helium core of  $M_{\text{He}} = 0.35M_{\odot}$ ),  $P = 228$  d, and the mass transfer rate of  $\dot{M}_2 \sim 1 \times 10^{-7}M_{\odot} \text{ yr}^{-1}$ . This set of the initial parameters is shown in Figure A11 by a star mark ( $\star$ ). It seems that T CrB is a critical (failing/succeeding) system for SN Ia explosion because this initial model corresponds to the lower boundary of the SN Ia region for  $M_{\text{WD},0} = 1.0M_{\odot}$  (Fig. A11). It should be noted here that a recent analysis by Belczyński & Mikolajewska (1998) shows, contrary to the previous results (e.g., Webbink et al. 1987), the mass ratio of T CrB to be  $q = M_{\text{RG}}/M_{\text{WD}} \sim 0.6$ , which implies a low-mass binary system and is very consistent with the present numerical results.

For RS Oph, if we start the calculation with  $M_{\text{WD},0} = 1.0M_{\odot}$ ,  $M_{\text{RG},0} = 1.15M_{\odot}$ , and  $P_0 = 240$  d, we obtain the present state of  $M_{\text{WD}} = 1.36M_{\odot}$ ,  $M_{\text{RG}} = 0.60M_{\odot}$  (with a helium core of  $M_{\text{He}} = 0.39M_{\odot}$ ),  $P = 460$  d, and the mass transfer rate of  $\dot{M}_2 \sim 1 \times 10^{-7}M_{\odot} \text{ yr}^{-1}$ . RS Oph also seems to be a critical system for SN Ia explosion. It should be noted that these sets of the initial parameters are not unique.

U Scorpii (U Sco) is also one of the well-known recurrent novae. Light curve fitting indicates a very massive white dwarf of  $M_{\text{WD}} = 1.37 - 1.38M_{\odot}$  (Kato 1990, 1995, 1999). The orbital period is  $P = 1.23$  d (Schaefer & Ringwald 1995), thus corresponding to the WD+MS system. Observations have suggested that the companion of U Sco is extremely helium-rich (e.g., Williams et al. 1981), although its companion is a slightly evolved main-sequence star (Schaefer 1990; Johnston & Kulkarni 1992). Its evolutionary path has long been regarded as a puzzle in the theory of close binary evolution (e.g., Webbink et al. 1987). Very recently, Hachisu & Kato (1999b) have elucidated the reason why its companion has a helium-rich envelope and,

at the same time, why the white dwarf is so massive as the Chandrasekhar mass limit.

In Hachisu & Kato's (1999b) U Sco scenario, they start from a progenitor binary system of  $\sim 7-8M_\odot$  and  $\sim 2M_\odot$  stars with the initial separation of  $\sim 500 R_\odot$ . The primary component has first evolved to fill its Roche lobe when the helium core grows to  $\sim 1.4-1.6M_\odot$ . The binary undergoes a common envelope evolution and shrinks to the separation of  $\sim 10R_\odot$  between the naked helium core and the  $\sim 2M_\odot$  main-sequence star. The helium core evolves to fill its Roche lobe and stably transfers almost pure helium onto the secondary because of the mass ratio  $M_1/M_2 \lesssim 0.79$ . As a result, the secondary becomes a helium-rich star.

After the helium envelope of the primary is exhausted, the primary becomes a carbon-oxygen (C+O) white dwarf of  $0.9-1.0M_\odot$  and the secondary grows in mass to  $\sim 2.5M_\odot$ . When the secondary slightly evolves to fill its Roche lobe, it transfers helium-rich matter onto the C+O white dwarf on a thermal time scale. The white dwarf burns hydrogen atop the surface at a critical rate of  $\dot{M}_{\text{cr}} \sim 2.0 \times 10^{-6} (M_{\text{WD}}/M_\odot - 0.40) M_\odot \text{ yr}^{-1}$  for helium-rich matter and blows excess matter in winds. The white dwarf now grows to near the Chandrasekhar mass limit and the mass transfer rate decreases to a few to several times  $10^{-7} M_\odot \text{ yr}^{-1}$ . These pictures seem to be very consistent with the present distinct observational aspects of U Sco.

To summarize, the recurrent novae seem to be a critical system for SN Ia explosion. Recurrent novae are morphologically divided into three groups; dwarf companion, slightly evolved main-sequence companion, and red-giant companion (e.g., Schaefer & Ringwald 1995). T CrB ( $P_{\text{orb}} = 228$  d) and RS Oph ( $P_{\text{orb}} = 460$  d) belong to the last group of red-giant companion. U Sco ( $P_{\text{orb}} = 1.23$  d; Schaefer & Ringwald 1995) and V394 CrA ( $P_{\text{orb}} = 0.758$  d; Schaefer 1990) belong to the middle group of the slightly evolved main-sequence companions. Two of the three subgroups of the recurrent novae correspond to our progenitors (WD+MS/WD+RG systems). This close relation between the recurrent novae and our progenitors strongly support our scenario of SN Ia progenitors.

#### 4.2. Yungelson & Livio's criticism

Based on the population synthesis analysis, Yungelson & Livio (1998) claimed that almost no realization frequency is derived for the original HKN96's WD+RG model. First, we briefly explain their analysis why the original model by HKN96 does not produce enough number of SNe Ia. Second, we point out that very wide binaries with the initial separation of  $a_i \gtrsim 1500 R_\odot$ , which were not included in Yungelson & Livio's (1998) analysis, are essentially important in our SN Ia modeling.

A more massive component (mass of  $M_{1,i}$ ) of a binary first evolves to a red-giant (AGB stage) and fills its inner critical Roche lobe. After a common envelope phase, the more massive component leaves a C+O WD and the separation of the binary decreases by a factor of

$$\frac{a_f}{a_i} \sim \alpha_{\text{CE}} \left( \frac{M_{\text{WD}}}{M_{1,i}} \right) \left( \frac{M_2}{M_{1,i} - M_{\text{WD}}} \right), \quad (36)$$

where  $\alpha_{\text{CE}}$  is the efficiency factor of common envelope

evolutions,  $a_f$  ( $a_i$ ) the final (initial) separation, and  $M_2$  the mass of the secondary. Adopting a standard value of  $\alpha_{\text{CE}} = 1$ , we obtain  $a_f/a_i \sim 1/40-1/50$  for  $M_{\text{WD}} \sim 1 M_\odot$  and  $M_2 \sim 1 M_\odot$ , because a  $\sim 1 M_\odot$  WD descends from a main-sequence star of  $M_{1,i} \sim 7-8 M_\odot$  (e.g., Weidemann 1986; Yungelson et al. 1995). Yungelson & Livio (1998) assumed that the separation of interacting binaries is *smaller than*  $a_i \lesssim 1500 R_\odot$ . Then, the most wide binaries has the separation of  $a_f \lesssim 30-40 R_\odot$  after the common envelope evolution. Its orbital period is  $P_0 \lesssim 20$  d for  $M_{\text{WD},0} \sim 1 M_\odot$  and  $M_{\text{RG},0} \sim 1 M_\odot$ . There is no SN Ia region of the WD+RG systems for  $P_0 \lesssim 20$  d as seen from Figure A11. Thus, they concluded that we cannot expect any SN Ia explosions from the right SN Ia region (WD+RG system) of Figure A11.

If the WD+RG evolution starts only from an initial condition of  $P_0 \lesssim 20$  d and  $M_{\text{WD},0} \sim 1M_\odot$ , however, the present states of T CrB or RS Oph cannot be reached because of low mass transfer rates of  $|\dot{M}_t| \lesssim 1 \times 10^{-7} M_\odot \text{ yr}^{-1}$  (see also Figs. A11 and A12). Thus, the existence of recurrent novae T CrB and RS Oph seems to be against the above Yungelson & Livio's conjecture. The reason why T CrB or RS Oph are failed to be reproduced in Yungelson & Livio's modeling is due to their assumption of  $a_i \lesssim 1500 R_\odot$ . In what follows, we show that such wide WD+RG binaries as  $P_0 \sim 100-1000$  d are born from initially very wide binaries with  $a_i \sim 1500-40000 R_\odot$ .

A star with the zero-age main-sequence mass of  $M_{1,i} \lesssim 8 M_\odot$  ends up its life by ejecting its envelope in a wind of relatively slow velocities ( $v \sim 10-40 \text{ km s}^{-1}$ ). These wind velocity is as low as the orbital velocity of binaries with the separation of  $a_i \sim 1500-40000 R_\odot$  for  $M_{1,i} \sim 7 M_\odot$  and  $M_{2,i} \sim 1 M_\odot$ . When the wind velocity is as low as the orbital velocity, the numerical factor  $\ell_w$  in equation (11) increases to

$$\ell_w \approx 1.7 - 0.55 \left( \frac{v}{a\Omega_{\text{orb}}} \right)^2, \quad (37)$$

mainly because outflowing matter can get angular momentum from the binary motion by torque during its journey (see Appendix A). Here,  $v$  is the radial component of the wind velocity near the inner critical Roche lobe and the limiting case of  $\ell_w = 1.7$  for  $v = 0$  was obtained by Nariai (1975) and Nariai & Sugimoto (1976) for a test particle simulation ejecting from the outer Lagrangian points and Sawada, Hachisu, & Matsuda (1984) for a 2-D (equatorial plane) hydrodynamical simulation blowing a very slow wind from the primary surface which fills the inner critical Roche lobe.

Combining the two expressions, we obtain

$$\ell_w \approx \max \left[ 1.7 - 0.55 \left( \frac{v}{a\Omega_{\text{orb}}} \right)^2, \left( \frac{q}{1+q} \right)^2 \right], \quad (38)$$

which is a good approximation to  $\ell_w$  in the region of the wind velocity from zero to infinity. Switching from equation (12) to equation (37) occurs at  $v \sim 1.5a\Omega_{\text{orb}}$  for  $q = 2$ .

If we assume that slow winds blow from the primary and the mass of the secondary does not change ( $\dot{M}_2 = 0$ ), the separation is calculated from

$$\frac{\dot{a}}{a} = \frac{\dot{M}_1 + \dot{M}_2}{M_1 + M_2} - 2 \frac{\dot{M}_1}{M_1} - 2 \frac{\dot{M}_2}{M_2} + 2 \frac{\dot{J}}{J}$$



$$\begin{aligned}
 &= \left( 2\ell_w \frac{M_1 + M_2}{M_2} + \frac{M_1}{M_1 + M_2} - 2 \right) \frac{\dot{M}_1}{M_1} \\
 &\approx \left( 2\ell_w \frac{M_1}{M_2} - 1 \right) \frac{\dot{M}_1}{M_1}, \quad (M_1 \gg M_2). \quad (39)
 \end{aligned}$$

Therefore, the critical value of  $\ell_w$  is about  $0.5q = 0.5(M_2/M_1)$  for shrinking/expanding of the separation. When  $v \sim a\Omega_{\text{orb}}$ , the systemic loss of the angular momentum is estimated as  $\ell_w \approx 1.7 - 0.55(v/a\Omega_{\text{orb}})^2 \sim 1.0$  from equation (38). We therefore have  $\dot{a}/a \approx 2\dot{M}_1/M_2 < 0$ .

Once the binary system begins to shrink, its evolution becomes similar to a common envelope evolution (see *stages B-D* in Fig. A1). As the separation shrinks, the orbital velocity of  $a\Omega_{\text{orb}}$  increases. If the wind velocity is almost constant, the ratio of  $v/a\Omega_{\text{orb}}$  in equation (38) becomes smaller and smaller and the shrinking is accelerated more and more. Thus, the separation is reduced by a factor of  $1/40 - 1/50$ , i.e.,  $a_f \sim 30 - 1000 R_\odot$  for  $M_{1,i} \sim 7 M_\odot$  and  $M_{2,i} \sim 1 M_\odot$ . The orbital period becomes  $P_0 \sim 15 - 3000$  d for  $M_{\text{WD},0} \sim 1 M_\odot$  and  $M_2 \sim 1 M_\odot$  (*stage D* in Fig. A1). These initial sets of the parameters are very consistent with the initial conditions of our WD+RG progenitor systems.

To summarize, we must include binaries with the separation of

$$a_i \lesssim 5500 R_\odot \left( \frac{\xi}{1.7} \right)^2 \left( \frac{M_{1,i} + M_{2,i}}{M_\odot} \right) \left( \frac{10 \text{ km s}^{-1}}{v} \right)^2, \quad (40)$$

into the category of *interacting binaries*, where  $v$  is the velocity of slow wind (super wind) at the end of AGB evolution and  $\xi \sim 1.5 - 1.7$  is a numerical factor defined by

$$\xi^2 \equiv 3.0 - 0.9 \frac{q(1+2q)}{(1+q)^2}. \quad (41)$$

Here, we take the critical wind velocity of shrinking/expanding as

$$v_{\text{cr}} = \xi a \Omega_{\text{orb}}, \quad (42)$$

at the beginning of super wind phase.

#### 4.3. SN Ia frequency

We estimate the SN Ia rate in our Galaxy coming from our WD+RG/WD+MS systems by using equation (1) of Iben & Tutukov (1984), i.e.,

$$\nu = 0.2 \cdot \Delta q \cdot \int_{M_A}^{M_B} \frac{dM}{M^{2.5}} \cdot \Delta \log A \text{ yr}^{-1}, \quad (43)$$

where  $\Delta q$ ,  $\Delta \log A$ ,  $M_A$ , and  $M_B$  are the appropriate ranges of the mass ratio, of the initial separation, and the lower and the upper limits of the primary mass for SN Ia explosions in solar mass units, respectively. The estimated rate of the WD+RG/WD+MS systems is close to the observed rate in our Galaxy,  $\nu \sim 0.003 \text{ yr}^{-1}$  (e.g., Cappellaro et al. 1997; see also Yungelson & Livio 1998), as will be shown below.

#### 4.4. WD+RG systems

For the WD+RG progenitors, we assume that the initial region of the separation includes  $a_i \sim 1500 - 40000 R_\odot$

as well as  $a_i \lesssim 1500 R_\odot$  (see discussions above in §4.2). Dividing the initial white dwarf mass of  $M_{\text{WD},0}$  into four intervals, i.e.,  $0.8 - 0.9 M_\odot$ ,  $0.9 - 1.0 M_\odot$ ,  $1.0 - 1.1 M_\odot$ , and  $1.1 - 1.2 M_\odot$ , we estimate the realization frequencies. The mass range of  $M_{\text{WD},0} < 0.7 M_\odot$  is not included because no SN Ia explosions are expected for such low initial mass WDs. We omit the range of  $M_{\text{WD},0} = 0.7 - 0.8 M_\odot$  because its realization frequency is too small to contribute to the SN Ia rate as seen in Figures A12 and A13. To estimate the initial separation (or orbital period),  $\log A$ , and the initial lower/upper masses,  $M_A$  and  $M_B$ , of our WD+RG systems, we need to obtain the zero-age main sequence mass of the primary component ( $M_{1,i}$ ) and the contraction factor after the first common envelope phase. In single star evolutions,  $0.7 - 1.2 M_\odot$  white dwarfs descend from stars with the zero-age main sequence mass of  $M_i \sim 3 - 8 M_\odot$ , i.e.,  $M_A \sim 3 M_\odot$  and  $M_B \sim 8 M_\odot$ . More precisely, using Yungelson et al.'s (1995) equation (11) gives the final core mass (C+O WD mass) vs. the zero-age main sequence mass relation,

$$\log \frac{M_{\text{C+O}}}{M_\odot} = -0.22 + 0.36 \left( \log \frac{M_0}{M_\odot} \right)^{2.5}, \quad (44)$$

as numerically summarized in Table A4, where  $M_{\text{WD},0} = M_{\text{C+O}}$ . The initial separation should be larger than

$$a_i > \frac{R_1(\text{AGB})}{f(M_{1,i}/M_{2,i})} \approx 2R_1(\text{AGB}), \quad (45)$$

in order that the C+O core grows up to  $M_{\text{C+O}} = M_{\text{WD},0}$ . Here  $f(q) \approx 0.5$  for  $q \equiv M_{1,i}/M_{2,i} \sim 2 - 7$  and the radius of stars at the AGB phase is given by

$$\frac{R_1(\text{AGB})}{R_\odot} = 1050 \left( \frac{M_{\text{C+O}}}{M_\odot} - 0.5 \right)^{0.68}, \quad (46)$$

(Iben & Tutukov 1984). For example, the initial separation should be larger than  $a_i \sim 1,200 R_\odot$  for  $M_{\text{WD},0} = 1.0 M_\odot$  as summarized in Table A4.

For the binary of  $M_{\text{WD},0} = 1.0 M_\odot$  and  $M_{2,i} = 1 M_\odot$ , the contraction factor is estimated to be  $1/37$  by assuming the common envelope efficiency factor of  $\alpha_{\text{CE}} = 1$ . The range of the separation after common envelope evolution becomes  $a_f \sim 32 - 1,120 R_\odot$  (corresponding to  $P_0 \sim 15 - 3,070$  d) because of  $a_i \sim 1,200 - 41,700 R_\odot$  as summarized in Table A4. The orbital period of  $P_0 \sim 15 - 3,070$  d covers the SN Ia region (WD+RG system) of Figure A11. The binary parameters for other  $M_{\text{WD},0}$  are summarized in Table A4. The regions of the orbital period,  $\log P_0$ , also covers the SN Ia region (WD+RG system) of Figure A12. Here we assume  $v = 10 \text{ km s}^{-1}$  and  $v < v_{\text{cr}} = \xi a \Omega_{\text{orb}}$  to meet the condition for the binary to contract (§4.2). Since the region of  $\log A$  ( $\log a_i$ ) is shifted in parallel to the region of  $\log a_f$  by the contraction factor, the probability frequency for  $\Delta \log A$  is the same as for  $\Delta \log a_f$ . Then we approximately set as

$$\Delta \log A \approx \Delta \log P_0 \cdot \frac{2}{3}, \quad (47)$$

where  $\Delta \log P_0$  is taken from the SN Ia region in Figure A12 and the factor of  $2/3$  comes from the conversion between the period and the separation. Substituting  $\Delta \log A = 0.6 \cdot 2/3$ ,  $\Delta q = 2.6/4.48 - 1.2/5.60 = 0.37$ ,  $M_A = 4.48$ ,  $M_B = 5.60$ , we obtain  $\nu_{\text{WD},0.8-0.9} = 0.0006$ .

The SNe Ia rates for other WD mass intervals are summarized in Table A5. Then, the summation of SN Ia rates for three intervals ( $0.8 - 0.9M_{\odot}$ ,  $0.9 - 1.0M_{\odot}$ , and  $1.0 - 1.1M_{\odot}$ ) gives  $\nu_{\text{RG}} = 0.0017 \text{ yr}^{-1}$ , which is large enough to explain the dominant part of the SN Ia rate in our Galaxy. If we further include the WD mass range of  $M_{\text{WD},0} = 1.1 - 1.2M_{\odot}$ , which is not shown in Table A5, the realization frequency increases to  $\nu_{\text{RG}} = 0.0022 \text{ yr}^{-1}$ . Here, we have not shown the region for  $M_{\text{WD},0} = 1.2M_{\odot}$  in Figure A12 because Webbink et al.'s (1983) empirical formula is valid for  $M_{2,0} < 2.5 - 3.0M_{\odot}$  with a degenerate helium core. The range of  $M_{\text{WD},0} = 1.2M_{\odot}$  exceeds this limit.

To examine the effect of the stripping parameter,  $\eta_{\text{eff}}$ , we estimate the realization frequency for  $\eta_{\text{eff}} = 0.3$  as summarized in Table A6. The parameter region shrinks to one third in area compared with the case of  $\eta_{\text{eff}} = 1$ , so that the realization frequency is reduced to about one third of  $\eta_{\text{eff}} = 1$  case, i.e.,  $\nu_{\text{RG}} = 0.0008 \text{ yr}^{-1}$ .

#### 4.5. WD+MS systems

For the WD+MS progenitors, HKNU98 have found a new evolutionary path, which has not been taken into account in the previous works (e.g., Rappaport et al. 1994; Di Stefano & Rappaport 1994; Yungelson et al. 1996; Yungelson & Livio 1998), and estimated the realization frequency to be as large as  $\nu_{\text{MS}} = 0.001 \text{ yr}^{-1}$ . We briefly follow their new evolutionary path in the following and discuss the total rate of SN Ia explosions: If a  $\sim 1M_{\odot}$  C+O WD is descending from an AGB star, its zero-age main sequence mass is  $\sim 7M_{\odot}$  by equation (44) and the binary separation is larger than  $a_i \sim 1350 R_{\odot}$  if the secondary mass is  $\sim 2M_{\odot}$ . Its separation shrinks to  $a_f \sim 70 R_{\odot}$  after the common envelope evolution with  $\alpha_{\text{CE}} = 1$  (the secondary mass of  $\sim 2M_{\odot}$ ). Then the orbital period becomes  $P_0 \sim 40 \text{ d}$  and too long to become an SN Ia as seen in Figure A11. Therefore, the C+O WD comes not from an AGB star having the radius of equation (46) but from a helium star whose hydrogen-rich envelope has been stripped away in the first common envelope evolution (at the red-giant phase with a helium core). Then, we follow the evolution of a binary consisting of a helium star and a main-sequence star.

To estimate the decrease in the separation after the common envelope phase, we use the radius to helium core mass ( $R_1 - M_{1,\text{He}}$ ) relation, which are taken from tables given by Bressan et al. (1993). As an example, let us consider a pair of  $7M_{\odot} + 2.5M_{\odot}$  with the initial separation of  $a_i \sim 50 - 600R_{\odot}$ . The binary evolves to SN Ia through the following stages:

- 1) When the mass of the helium core grows to  $1.0M_{\odot} < M_{1,\text{He}} < 1.4M_{\odot}$ , the primary fills its Roche lobe and the binary undergoes a common envelope evolution.
- 2) After the common envelope evolution, the system consists of a helium star and a main-sequence star with a relatively compact separation of  $a_f \sim 3 - 40 R_{\odot}$  and  $P_{\text{orb}} \sim 0.4 - 20 \text{ d}$ .
- 3) The helium star contracts and ignites central helium burning to become a helium main-sequence star. The primary stays at the helium main-sequence for  $\sim 1 \times 10^7 \text{ yr}$  (e.g., Paczynski 1971).

- 4) After helium exhaustion, a carbon-oxygen core develops. When the core mass reaches  $0.9 - 1.0M_{\odot}$ , the helium star evolves to a red-giant and fills again its inner critical Roche lobe. Almost pure helium is transferred to the secondary because the mass transfer is stable for the mass ratio  $q = M_1/M_2 < 0.79$ . The mass transfer rate is as large as  $\sim 1 \times 10^{-5}M_{\odot} \text{ yr}^{-1}$  but the mass-receiving main-sequence star ( $\sim 2 - 3M_{\odot}$ ) does not expand for such a low rate (e.g., Kippenhahn & Meyer-Hofmeister 1977).
- 5) The secondary has received  $0.1 - 0.4M_{\odot}$  (almost) pure helium and, as a result, it becomes a helium-rich star as observed in U Sco (e.g., Williams et al. 1981; Barlow et al. 1981; Hanes 1985; Sekiguchi et al. 1988). The separation and thus the orbital period gradually increases during the mass transfer phase. The final orbital period becomes  $P_{\text{orb}} \sim 0.5 - 40 \text{ d}$ .
- 6) An SN Ia explosion occurs when  $P_0 = 0.4 - 5 \text{ d}$  and  $M_2 = M_{\text{MS},0} \sim 2 - 3M_{\odot}$  in the  $\log P_0 - M_{\text{d},0}$  plane for the system of  $M_1 = M_{\text{WD},0} \sim 0.9 - 1.0M_{\odot}$  as seen in Figure A12.

Therefore, the above pair of  $7M_{\odot} + 2.5M_{\odot}$  can be a progenitor of SNe Ia if the initial separation is between  $50 - 150R_{\odot}$ , which initiates a common envelope evolution at the helium core mass of  $M_{1,\text{He}} = 1.0 - 1.2M_{\odot}$ , corresponding to the initial orbital period of  $P_{\text{orb},0} = 0.5 - 5 \text{ d}$  for the WD+MS systems in Figure A11. In this case, we have  $\Delta \log A = \log 150 - \log 50 = 0.5$  and  $q = 2.5/7 = 0.36$  in equation (43).

Calculating 25 pairs of  $M_{1,i}$  and  $M_{2,i}$ , HKNU99 have obtained the parameter region of SN Ia explosion as  $\Delta q = 0.4$ ,  $\Delta \log A = 0.5$ ,  $M_A = 5.5$ , and  $M_B = 8.5$ . Substituting these values into equation (43), we obtain the SN Ia rate of  $\nu_{\text{MS}} = 0.001 \text{ yr}^{-1}$ . Thus HKNU99 have shown that the frequency of the WD+MS systems is about one third of the inferred rate in our Galaxy, which is much larger than that of Yungelson & Livio's (1998) estimation. It should be noted that Yungelson & Livio (1998) have obtained the birth rate of  $1 \times 10^{-3} \text{ yr}^{-1}$  for their models 15 and 16 by relaxing all the constraints on the mass ratio of their binary models, although it is not a realistic case.

The orbital velocity of the WD+MS systems is much faster than that for the WD+RG systems, i.e.,  $a\Omega_{\text{orb}} \sim 400 \text{ km s}^{-1}$  for  $M_{\text{WD}} = 1.0M_{\odot}$  and  $M_{\text{MS}} = 2.0M_{\odot}$  at the zero-age main sequence. Then, the switching from equation (12) to equation (37) occurs at  $v \sim 1.5a\Omega_{\text{orb}} \sim 600 \text{ km s}^{-1}$ . This means that the wind velocity has to be faster than  $\sim 600 \text{ km s}^{-1}$  in order to avoid the formation of a common envelope. Otherwise, winds carry large specific angular momentum and drastically shorten the separation to enhance the mass transfer and to eventually form a common envelope. Our strong winds satisfy the condition of  $v \gtrsim 600 \text{ km s}^{-1}$  and this supports Li & van den Heuvel's evolutionary process and also HKNU99's modeling on the WD+MS systems.

To summarize, the contribution of the WD+MS systems to the SN Ia rate in our Galaxy is about one third of the inferred rate in our Galaxy. The total SN Ia rate of the WD+MS/WD+RG systems becomes  $\nu_{\text{RG+MS}} = \nu_{\text{RG}} + \nu_{\text{MS}} = 0.003 \text{ yr}^{-1}$ , which is close enough to the inferred rate of our Galaxy.

#### 4.6. Observational detection of hydrogen

In our scenario, the WD winds form a circumstellar envelope around the binary systems prior to the explosion, which may emit X-rays, radio, and H $\alpha$  lines by shock heating when the ejecta collide with the circumstellar envelope. In HKN96's model of binary evolution, the mass accretion rate decreases well below  $1 \times 10^{-6} M_{\odot} \text{ yr}^{-1}$  as the white dwarf mass gets close to the Chandrasekhar limit. Thus the strong wind has ceased when the white dwarf explodes (HKN96). In contrast, the mass accretion rate in the present models is still as high as  $1 \times 10^{-6} M_{\odot} \text{ yr}^{-1}$  for some of the white dwarfs near the Chandrasekhar limit, so that such a white dwarf explodes in the strong wind phase.

Our strong wind model of case P1 predicts the presence of circumstellar matter around the exploding white dwarf. Whether such a circumstellar matter is observable depends on its density. The wind mass loss rate from the white dwarf near the Chandrasekhar limit is as high as  $\dot{M} \sim 1 \times 10^{-8} - 1 \times 10^{-7} M_{\odot} \text{ yr}^{-1}$  and the wind velocity is  $v = 1000 \text{ km s}^{-1}$  (Fig. A5). Despite the relatively high mass loss rate, the circumstellar density is not so high because of the high wind velocity. For steady wind, the density is expressed by  $\dot{M}/v$  ( $= 4\pi r^2 \rho$ ). Normalized by the typical red-giant wind velocity of  $10 \text{ km s}^{-1}$ , the density measure of our white dwarf wind is given as  $\dot{M}/v_{10} \sim 1 \times 10^{-10} - 1 \times 10^{-9} M_{\odot} \text{ yr}^{-1}$ , where  $v_{10} = v/10 \text{ km s}^{-1}$ .

Behind the red-giant, matter stripped from the red-giant component forms a much dense circumstellar tail. Its rate is as large as  $\sim 1 \times 10^{-7} M_{\odot} \text{ yr}^{-1}$  with the velocity of  $\sim 100 \text{ km s}^{-1}$ . The density measure of the dense red-giant wind thus formed is  $\dot{M}/v_{10} \sim 1 \times 10^{-8} M_{\odot} \text{ yr}^{-1}$ .

Further out, circumstellar matter is produced from the wind from the red-giant companion, which is too far away to cause significant circumstellar interaction.

For cases P2 and P3, winds from the WD have stopped before the explosion. Therefore, circumstellar matter is dominated by the wind from the red-giant companion whose velocity is as low as  $\sim 10 \text{ km s}^{-1}$ .

At SN Ia explosion, ejecta would collide with the circumstellar matter, which produces shock waves propagating both outward and inward. At the shock front, particle accelerations take place to cause radio emissions. Hot plasmas in the shocked materials emit thermal X-rays. The circumstellar matter ahead of the shock is ionized by X-rays and produce recombination H $\alpha$  emissions (Cumming et al. 1996). Such an interaction has been observed in Type Ib, Ic, and II supernovae, most typically in SN 1993J (e.g., Suzuki & Nomoto 1995 and references therein).

For SNe Ia, several attempts have been made to detect the above signature of circumstellar matter. There has been no radio and X-ray detections so far. The upper limit set by X-ray observations of SN 1992A is  $\dot{M}/v_{10} = (2 - 3) \times 10^{-6} M_{\odot} \text{ yr}^{-1}$  (Schlegel & Petre 1993). Radio observations of SN 1986G have provided the most strict upper limit to the circumstellar density as  $\dot{M}/v_{10} = 1 \times 10^{-7} M_{\odot} \text{ yr}^{-1}$  (Eck et al. 1995). This is still 10 – 100 times higher than the density predicted for the white dwarf wind for case P1. For cases P2 and P3, if the wind mass loss rate from the red-giant is significantly higher than  $1 \times 10^{-7} M_{\odot} \text{ yr}^{-1}$ , radio detection could be possible for very nearby SNe Ia as close as SN 1986G. (Note also that SN 1986G is not a typical SN Ia but a subluminous SN Ia.)

For H $\alpha$  emissions, Branch et al. (1983) noted a small, narrow emission feature at the rest wavelength of H $\alpha$ , which is blueshifted by  $1800 \text{ km s}^{-1}$  from the local interstellar Ca II absorption. Though this feature was not observed 5 days later, such high velocity hydrogen is expected from the white dwarf wind model. For SN 1994D, Cumming et al. (1996) obtained the upper limit of  $\dot{M}/v_{10} = 6 \times 10^{-6} M_{\odot} \text{ yr}^{-1}$ . Further attempts to detect H $\alpha$  emissions are highly encouraged (Lundqvist & Cumming 1997).

## 5. CONCLUSIONS

Progenitors of SNe Ia have not been identified yet either theoretically or observationally. In the present paper, we propose a new evolutionary process which produces a wide enough symbiotic channel to SNe Ia. In this channel, the white dwarf accreting mass from the lobe-filling evolved companion (red-giant) grows to the Chandrasekhar limit and explodes as an SN Ia. In what follows we summarize our main results:

1. In HKN96, we have found the most important mechanism in our symbiotic channel to SNe Ia: when the mass accretion rate onto the white dwarf exceeds a critical rate of  $\dot{M}_{\text{cr}} \approx 0.75 \times 10^{-6} (M_{\text{WD}}/M_{\odot} - 0.40) M_{\odot} \text{ yr}^{-1}$ , a strong optically thick wind blows from the white dwarf. It stabilizes the mass transfer even if the red-giant has a deep convective envelope. HKN96 have shown that the mass transfer becomes stable only when the mass ratio of RG/WD is smaller than 1.15. In the present study, we have found that this constraint is removed when the effect of mass-stripping from the red-giant envelope by the strong wind is large enough. Thus the symbiotic channel produces SNe Ia for a much (more than ten times) wider range of the binary parameters than that of HKN96's estimation, thus being able to account for the dominant part of the inferred rate of SNe Ia in our Galaxy. It should be noticed, however, that the realization frequency depends on the efficiency factor of mass-stripping  $\eta_{\text{eff}}$  and the realization frequency is consistent with the inferred rate in our Galaxy for  $\eta_{\text{eff}} \sim 0.3 - 1.0$ .
2. Yungelson & Livio (1998) estimated the realization frequency of HKN96's original model and concluded that almost no realization frequency is derived because the binary shrinks too much ( $P_{\text{orb}} < 20 \text{ d}$ ) to produce an SN Ia after the first common envelope evolution. In their population synthesis code, however, Yungelson & Livio (1998) assumed that the initial separation is *smaller than*  $\sim 1500 R_{\odot}$ , i.e.,  $a_i \lesssim 1500 R_{\odot}$ . This assumption neglects the effect of slow winds at the end of stellar evolution. When the velocity of the slow wind is as small as the orbital velocity, the slow wind gets angular momentum through torque by the binary motion and, as a result, the binary shrinks so much. When the wind velocity is as slow as  $\sim 10 \text{ km s}^{-1}$ , we must include the binaries with the separation of  $a_i \sim 1,500 - 40,000 R_{\odot}$ . Such an extremely wide binary will shrink to an appropriate range of the separation ( $20 \text{ d} < P_0 < 3000 \text{ d}$  for a pair of  $M_{\text{WD},0} \sim 1 M_{\odot}$  and  $M_{2,i} \sim 1 M_{\odot}$ ) after the slow wind (super wind) and the common

envelope evolution. If this effect is included in the calculation of SN Ia rate, we have a reasonable value of the realization frequency,  $\nu_{\text{RG}} = 0.002 \text{ yr}^{-1}$ , for our white dwarf plus red-giant (WD+RG) systems.

3. Yungelson & Livio (1998) estimated the realization frequency of Li & van den Heuvel's (1997) white dwarf plus main sequence star (WD+MS) model and concluded that the total frequency of their modified HKN96's model and Li & van den Heuvel's model does not exceed  $0.0002 \text{ yr}^{-1}$ , a tenth of the inferred rate. However, we believe that an important evolutionary path was not included in Yungelson & Livio's (1998) analysis, that is, the primary's helium star phase: the primary becomes a naked helium star after the first common envelope phase if the mass transfer begins at the phase of a red-giant with a helium core. This helium star eventually leaves a C+O WD by transferring the helium envelope to the secondary. As a result, the secondary may have an extremely helium-rich envelope such as in U Sco (e.g., Williams et al. 1981; Barlow et al. 1981; Hanes 1985; Sekiguchi et al. 1988). This evolutionary path indicates that the secondary of the WD+MS systems has a helium-enriched envelope thus forming an accretion disk which shows strong helium lines as seen in the luminous supersoft X-ray sources (e.g., Kahabka & van den Heuvel 1997 for a recent review). Including this evolutionary path in the estimation of SN Ia rate, HKNU99 have obtained a much larger frequency of  $\nu_{\text{MS}} = 0.001 \text{ yr}^{-1}$  for the WD+MS systems than that estimated by Yungelson & Livio (1998). Thus the total frequency of our WD+RG/WD+MS systems is as large as  $\nu = \nu_{\text{RG}} + \nu_{\text{MS}} = 0.003 \text{ yr}^{-1}$ , which is consistent with the inferred rate in our Galaxy.
4. Recurrent novae are morphologically divided into three groups; dwarf companion, slightly evolved main-sequence companion, and red-giant companion (e.g., Schaefer & Ringwald 1995). T CrB ( $P_{\text{orb}} = 228 \text{ d}$ ) and RS Oph ( $P_{\text{orb}} = 460 \text{ d}$ ) belong to the last group of red-giant companion. It has been argued that their white dwarf masses are very close to the Chandrasekhar mass limit. These systems correspond to near the lower boarder of our SN Ia region (WD+RG) as shown in Figure A11 and its evolutionary path is reasonably understood by our WD+RG

systems. On the other hand, U Sco ( $P_{\text{orb}} = 1.23 \text{ d}$ ) and V394 CrA ( $P_{\text{orb}} = 0.758 \text{ d}$ ) belong to the middle group of slightly evolved main-sequence companion. Our WD+MS model naturally yields a helium-enriched envelope of the secondary star as well as a near Chandrasekhar mass limit white dwarf as has been observationally suggested. The evolutionary path of the WD+MS systems is also very consistent with the middle group of recurrent novae.

5. The immediate progenitors in our symbiotic channel to SNe Ia may be observed as a symbiotic star. The photospheric temperature of the mass-accreting white dwarf is kept around  $T_{\text{ph}} \sim 1 \times 10^5 - 2 \times 10^5 \text{ K}$  during the wind phase. The hot star may not be observed in X-rays during the strong wind phase due to self-absorption by the wind itself. Some progenitors stop blowing the wind before the SN Ia explosion, thus being observed as a luminous supersoft X-ray source. In some progenitors, very weak hydrogen shell flashes are triggered before the SN Ia explosion; such a progenitor may be observed as a recurrent nova like T CrB or RS Oph.
6. Radio emission from the circumstellar gas is predicted. If the white dwarfs explode in the strong wind phase, however, radio emission is lower than the current observational limit because the wind velocity is as fast as  $1000 \text{ km s}^{-1}$  and the density of the circumstellar medium is too tenuous to be observed even if the wind mass loss rate is as large as  $\sim 1 \times 10^{-6} M_{\odot} \text{ yr}^{-1}$  or more. If the wind has stopped before the explosion, the circumstellar matter is dominated by the low velocity wind from the red-giant companion; then observations of radio emission would be easier. Detection of high velocity hydrogen feature from the strong wind is also predicted.

We thank the referee, Mario Livio, for his helpful comments to improve the manuscript. We are also grateful to Lev Yungelson for his kind comments and corrections on the manuscript. This research has been supported in part by the Grant-in-Aid for Scientific Research (05242102, 06233101, 08640321, 09640325) and COE research (07CE2002) of the Japanese Ministry of Education, Science, Culture, and Sports.

## APPENDIX

### SPECIFIC ANGULAR MOMENTUM OF WINDS

To obtain the relation between  $v/a\Omega_{\text{orb}}$  and  $\ell_{\text{w}}$  in equations (11) and (39), we calculate many orbits of test particles moving under the Roche potential and Coriolis force, i.e.,

$$\begin{aligned}
 \frac{d^2x}{dt^2} &= 2 \frac{dy}{dt} + x - \frac{1}{1+q} \frac{x-x_1}{r_1^3} - \frac{q}{1+q} \frac{x-x_2}{r_2^3}, \\
 \frac{d^2y}{dt^2} &= -2 \frac{dx}{dt} + y - \frac{1}{1+q} \frac{y}{r_1^3} - \frac{q}{1+q} \frac{y}{r_2^3}, \\
 \frac{d^2z}{dt^2} &= -\frac{1}{1+q} \frac{z}{r_1^3} - \frac{q}{1+q} \frac{z}{r_2^3},
 \end{aligned} \tag{A1}$$

where  $(x, y, z)$  is the position of the particle,  $q = M_2/M_1$  the mass ratio,  $r_1$  and  $r_2$  are the distances from the primary and from the secondary to the test particle, respectively, and calculated from

$$\begin{aligned} r_1^2 &= (x - x_1)^2 + y^2 + z^2, \\ r_2^2 &= (x - x_2)^2 + y^2 + z^2. \end{aligned} \quad (\text{A2})$$

Setting the center of gravity of the binary at the origin of the coordinates, we assume that the primary is located on the negative side of the x-axis  $(x_1, 0, 0)$  and the secondary is located on the positive side of the x-axis  $(x_2, 0, 0)$ , i.e.,

$$\begin{aligned} x_1 &= -\frac{q}{1+q}, \\ x_2 &= \frac{1}{1+q}. \end{aligned} \quad (\text{A3})$$

We also assume  $a = 1$ ,  $G = 1$ , and  $\Omega_{\text{orb}} = 1$  (or  $M_1 + M_2 = 1$ ) in our dimensionless form.

The primary (AGB star) blows spherically symmetric winds with the initial velocity of  $v_0$ . This process can be simulated by ejecting test particles from the primary surface at the radius which is much smaller than the inner critical Roche lobe, e.g., one tenth of the inner critical Roche lobe of the primary; i.e., we set

$$v = v_0, \quad \text{at } r_1 = 0.1R_1^*. \quad (\text{A4})$$

The trajectory of the wind may be approximated by a trajectory of the particle with the same initial velocity and position when the wind is supersonic and does not form a shock. Here, we assume the equatorial symmetry of the wind. Dividing the primary surface into  $64 \times 256$  parts, i.e., the azimuthal angle (from  $\phi = 0$  to  $\phi = 2\pi$ ) into 256, ( $\Delta\phi = 2\pi/256$ ), and the inclination angle (from  $\theta = 0$  to  $\theta = \pi/2$ ) into 64 ( $\Delta\theta = \pi/2/64$ ), we eject test particles from each center of the surface elements with the initial radial velocity of  $v_0$ . We attach the mass loss rate of  $v_0 \sin\theta_i \Delta\theta \Delta\phi / 4\pi$  to each particle.

The radial component of the wind velocity  $v_r$  near the inner critical Roche lobe is calculated from

$$v_r = 2 \sum_i \frac{1}{r_1} \left( \frac{dx_i}{dt} (x_i - x_1) + \frac{dy_i}{dt} y_i + \frac{dz_i}{dt} z_i \right) \frac{\sin\theta_i \Delta\theta \Delta\phi}{4\pi}, \quad \text{at } r_{1,i} = R_1^*, \quad (\text{A5})$$

where the position of each test particle is denoted by  $(x_i, y_i, z_i)$  and the *radial* means the direction from the center of the primary to the test particle. We estimate the average specific angular momentum of the test particles by

$$\ell_w = 2 \sum_i \left( x_i^2 + y_i^2 + x_i \frac{dy_i}{dt} - y_i \frac{dx_i}{dt} \right) \frac{\sin\theta_i \Delta\theta \Delta\phi}{4\pi} / 2 \sum_i \frac{\sin\theta_i \Delta\theta \Delta\phi}{4\pi}, \quad \text{at } r_i = 10. \quad (\text{A6})$$

It should be noted that some test particles are trapped to the secondary and never reach the radius of  $r = 10$  when the radial velocity is smaller than the orbital velocity, i.e.,  $v_r < a\Omega_{\text{orb}} = 1$ . We do not include these particles in the calculation of the specific angular momentum of the wind in equation (A6).

The integration of equation (A1) is based on the second order leap-frog method. Five cases of the mass ratio,  $q = M_2/M_1 = 3, 2, 1, 1/2,$  and  $1/3$ , are calculated for various initial velocity  $v_0$ . The relation between the specific angular momentum  $\ell_w$  and the radial velocity near the inner critical Roche lobe of the primary  $v$  ( $\equiv v_r$ ) is plotted in Figure A14. When the radial velocity of the wind is faster than twice the orbital velocity, i.e.,  $v \gtrsim 2$  (or  $v \gtrsim 2a\Omega_{\text{orb}}$ ), the specific angular momentum is approximated by the limiting value of equation (12) for very fast winds. For wind velocities lower than 2, the specific angular momentum rapidly increases. We find that the values are located approximately on a quadratic line of

$$\ell_w \approx 1.7 - 0.55v^2, \quad (\text{A7})$$

where the limiting case of  $\ell_w = 1.7$  for  $v = 0$  was obtained by Nariai (1975) and Nariai & Sugimoto (1976) for a test particle simulation and Sawada et al. (1984) for a two-dimensional (equatorial plane) hydrodynamic simulation. Thus, the specific angular momentum is approximated by

$$\ell_w \approx \max \left[ 1.7 - 0.55 \left( \frac{v}{a\Omega_{\text{orb}}} \right)^2, \left( \frac{q}{1+q} \right)^2 \right], \quad (\text{A8})$$

at least for these five different mass ratios, although three-dimensional hydrodynamic calculations should be done in order to obtain a definite conclusion of the specific angular momentum of the winds.

## REFERENCES

- Arnett, W.D. 1996, *Nucleosynthesis and Supernovae* (Princeton: Princeton Univ. Press)
- Barlow, M. J., et al. 1981, *MNRAS*, 195, 61
- Belczyński, K., & Mikolajewska, J. 1998, *MNRAS*, 296, 77
- Branch, D. 1998, *Ann. Rev. Astron. Astrophys.* 36, 17
- Branch, D., Lacy, C.H., McCall, M.L., Sutherland, P., Uomoto, A., Wheeler, J.C., & Wills, B.J. 1983, *ApJ*, 270, 123
- Branch, D., Livio, M., Yungelson, L.R., Boffi, F.R., & Baron, E. 1995, *PASP*, 107, 717
- Bressan, A., Fagotto, F., Bertelli, G., & Chiosi, C. 1993, *A&AS*, 100, 647
- Cappellaro, E., Turatto, M., Tsvetkov, D. Yu., Bartunov, O. S., Pollas, R., Evans, R., & Hamuy, M. 1997, *A&A*, 322, 431
- Cumming, R.J., Lundqvist, P., Smith, L.J., Pettini, M., & King, D.L. 1996, *MNRAS*, 283, 1355
- Di Stefano, R., & Rappaport, S. 1994, *ApJ*, 437, 733
- Dobrzycka, D. & Kenyon, S. J. 1994, *AJ*, 108, 2259
- Eck, C.R., Cowan, J.J., Roberts, D.A., Boffi, F.R., & Branch, D. 1995, *ApJ*, 451, L53
- Eggleton, P. P. 1983, *ApJ*, 268, 368
- Hachisu, I., & Kato, M. 1999a, *ApJ*, 517, in press (astro-ph/9903254)
- Hachisu, I., & Kato, M. 1999b, *ApJ*, submitted
- Hachisu, I., Kato, M., & Nomoto, K. 1996, *ApJ*, 470, L97 (HKN96)
- Hachisu, I., Kato, M., Nomoto, K., & Umeda, H. 1999, *ApJ*, 519, in press (HKN99) (astro-ph/9902303)
- Hanes, D. A. 1985, *MNRAS*, 213, 443
- Höflich, P., & Khokhlov, A. 1996, *ApJ*, 457, 500
- Iben, I. Jr. 1988, *ApJ*, 324, 355
- Iben, I. Jr., & Livio, M. 1993, *PASP*, 105, 1373
- Iben, I. Jr., & Tutukov, A. V. 1984, *ApJS*, 54, 335
- Iben, I. Jr., & Tutukov, A. V. 1985, *ApJS*, 58, 661
- Iglesias, C. A., & Rogers, F. 1996, *ApJ*, 464, 943
- Johnston, H. M., & Kulkarni, S. R. 1992, *ApJ*, 396, 267
- Kahabka, P., & van den Heuvel, E. P. J. 1997, *ARA&A*, 35, 69
- Kato, M. 1990, *ApJ*, 355, 277
- Kato, M. 1991, *ApJ*, 369, 471
- Kato, M. 1995, in *Cataclysmic Variables*, eds. A. Bianchini, M. Della Valle, & M. Orio (Dordrecht: Kluwer), 243
- Kato, M. 1999, *PASJ*, submitted
- Kato, M., & Hachisu, I., 1994, *ApJ*, 437, 802
- Kato, M., & Hachisu, I., 1999, *ApJ*, 513, L41
- Kato, M., Saio, H., & Hachisu, I. 1989, *ApJ*, 340, 509
- Kenyon, S.J., Livio, M., Mikolajewska, J., & Tout, C.A. 1993, *ApJ*, 407, L81
- Kippenhahn, R., & Meyer-Hofmeister, E. 1977, *A&A*, 54, 539
- Kovetz, A., & Prialnik, D. 1994, *ApJ*, 424, 319
- Li, X.-D., & van den Heuvel, E. P. J. 1997, *A&A*, 322, L9
- Lines, H. C., Lines, R. D., & McFaul, T. G. 1988, *AJ*, 95, 1505
- Livio, M. 1996, in *Supersoft X-Ray Sources*, ed. J. Greiner (Berlin: Springer), p. 183
- Lundqvist, P. & Cumming, R.J. 1997, in *Advances in Stellar Evolution*, ed. R.T. Rood & A. Renzini (Cambridge: Cambridge University Press), 293
- Munari, U., & Renzini, A. 1992, *ApJ*, 397, L87
- Nariai, K. 1975, *A&A*, 43, 309
- Nariai, K., & Sugimoto, D. 1976, *PASJ*, 28, 593
- Nomoto, K. 1982, *ApJ*, 253, 798
- Nomoto, K., & Iben, I. Jr. 1985, *ApJ*, 297, 531
- Nomoto, K., Iwamoto, K., & Kishimoto, N. 1997, *Science*, 276, 1378
- Nomoto, K., & Kondo, Y. 1991, *ApJ*, 367, L19
- Nomoto, K., Nariai, K., & Sugimoto, D. 1979, *PASJ*, 31, 287
- Nomoto, K., Thielemann, F., & Yokoi, K. 1984, *ApJ*, 286, 644
- Nugent, P., Baron, E., Branch, D., Fisher, A., & Hauschildt, P. H. 1997, *ApJ*, 485, 812
- Paczynski, B. 1971, *Acta Astronomica*, 21, 1
- Rappaport, S., Di Stefano, R., & Smith, J. D. 1994, *ApJ*, 426, 692
- Renzini, A. 1996, in *IAU Colloquium 145, Supernovae and Supernova Remnants*, ed. R. McCray & Z. Wang (Cambridge: Cambridge University Press), 77
- Rogers, F. J., & Iglesias, C. A., 1992, *ApJS*, 79, 507
- Saio, H., & Nomoto, K. 1985, *A&A*, 150, L21
- Saio, H., & Nomoto, K. 1998, *ApJ*, 500, 388
- Sawada, K., Hachisu, I., & Matsuda, T. 1984, *MNRAS*, 206, 673
- Schaefer, B. 1990, *ApJ*, 355, L39
- Schaefer, B., & Ringwald, F. A. 1995, *ApJ*, 447, L45
- Schlegel, E.M., & Petre, R. 1993, *ApJ*, 418, L53
- Sekiguchi, K., Feast, M. W., Whitelock, P. A., Overbeek, M. D., Wargau, W., & Spencer Jones, J. 1988, *MNRAS*, 234, 281
- Segretain, L., Chabrier, G., & Mochkovitch, R. 1997, *ApJ*, 481, 355
- Selvelli, P. L., Cassatella, A., & Gilmozzi, R. 1992, *ApJ*, 393, 289
- Shahbaz, T., Somers, M., Yudin, B., & Naylor, T. 1997, *MNRAS*, 288, 1027
- Starrfield, S., Sparks, W. M., & Shaviv, G. 1988, *ApJ*, 325, L35
- Suzuki, T., & Nomoto, K. 1995, *ApJ*, 455, 658
- Webbink, R. F. 1984, *ApJ*, 277, 355
- Webbink, R. F., Livio, M., Truran, J. W., & Orio, M. 1987, *ApJ*, 314, 653
- Webbink, R. F., Rappaport, S., & Savonije, G. J. 1983, *ApJ*, 270, 678
- Weidemann, V. 1986, *Late Stages of Stellar Evolution*, ed. S. Kwok, & S. P. Pottasch (Dordrecht: Reidel), 347
- Whelan, J., & Iben, Jr. I. 1973, *ApJ*, 186, 1007
- Williams, R. E., Sparks, W. M., Gallagher, J. S., Ney, E. P., Starrfield, S. G., & Truran, J. W. 1981, *ApJ*, 251, 221
- Woosley, S.E. 1990, in *Supernovae*, ed. A.G. Petcheck (New York: Springer Verlag), 182
- Yungelson, L., & Livio, M. 1998, *ApJ*, 497, 168
- Yungelson, L., Livio, M., Truran, J. W., Tutukov, A., & Fedorova, A. 1996, *ApJ*, 466, 890
- Yungelson, L., Livio, M., Tutukov, A., & Kenyon, S. 1995, *ApJ*, 447, 656
- Yungelson, L., Tutukov, A., & Livio, M. 1993, *ApJ*, 418, 794

TABLE A1  
NUMERICAL FACTORS OF MASS-STRIPPING EFFECT

| $q$         | 0.5   | 1     | 2     | 3     | 5     |
|-------------|-------|-------|-------|-------|-------|
| $g(q)$      | 0.013 | 0.019 | 0.025 | 0.030 | 0.036 |
| $\ell_s(q)$ | 0.144 | 0.025 | 0.006 | 0.044 | 0.105 |

TABLE A2  
THREE TYPICAL CASES OF SN IA PROGENITOR EVOLUTION

| case | $M_{\text{WD},0}$<br>( $M_{\odot}$ ) | $M_{\text{RG},0}$<br>( $M_{\odot}$ ) | $P_0$<br>(day) | $\dot{M}_t$<br>( $M_{\odot} \text{ yr}^{-1}$ ) | $\dot{M}_w$<br>( $M_{\odot} \text{ yr}^{-1}$ ) | $M_s$<br>( $M_{\odot} \text{ yr}^{-1}$ ) |
|------|--------------------------------------|--------------------------------------|----------------|--|--|--|
| P1   | 1.0                                  | 2.0                                  | 300            | $-8.7 \times 10^{-7}$                          | $-4.8 \times 10^{-7}$                          | $-2.0 \times 10^{-6}$                    |
| P2   | 1.0                                  | 1.6                                  | 300            | $-6.2 \times 10^{-7}$                          | $-2.3 \times 10^{-7}$                          | $-1.0 \times 10^{-6}$                    |
| P3   | 1.0                                  | 1.3                                  | 300            | $-5.2 \times 10^{-7}$                          | $-1.3 \times 10^{-7}$                          | $-5.4 \times 10^{-7}$                    |

TABLE A3  
THREE STATES OF IMMEDIATE SN IA PROGENITORS

| case | history |   |      |   | SN Ia explosion |      |
|------|---------|---|------|---|-----------------|------|
| P1   | WIND    | → | WIND | → | WIND            | WIND |
| P2   | WIND    | → | WIND | → | SSS             | SSS  |
| P3   | WIND    | → | SSS  | → | RN              | RN   |

TABLE A4  
CONTRACTION FACTOR ( $\alpha_{\text{CE}} = 1$ )

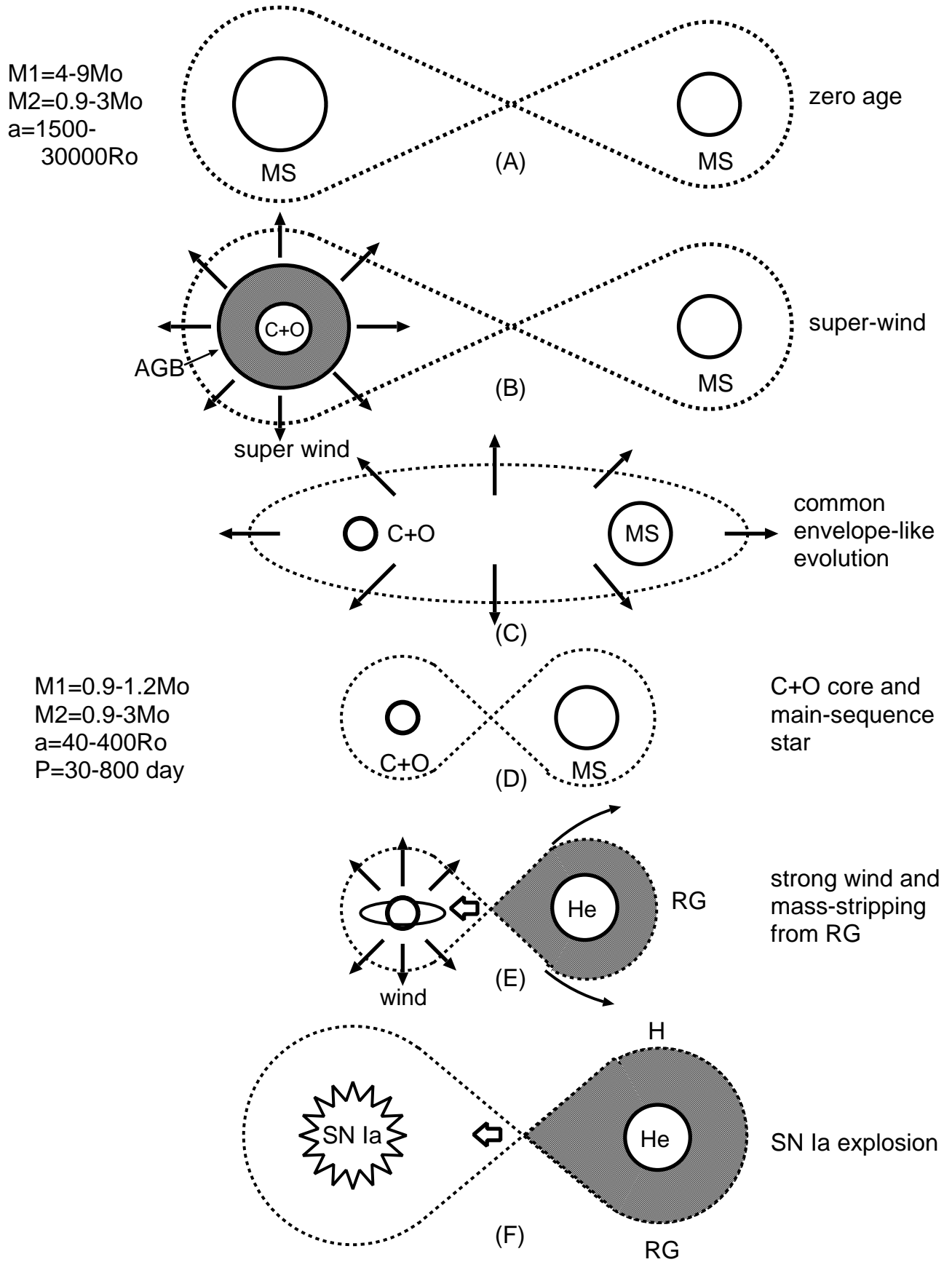
| $M_{\text{WD},0}$<br>( $M_{\odot}$ ) | $M_{1,0}$<br>( $M_{\odot}$ ) | $a_i$<br>( $R_{\odot}$ ) | $a_f$<br>( $R_{\odot}$ ) | $P_0$<br>(day) | $M_2$<br>( $M_{\odot}$ ) | contraction<br>factor |
|--------------------------------------|------------------------------|--------------------------|--------------------------|----------------|--------------------------|-----------------------|
| 0.7                                  | 3.20                         | 730 – 21,900             | 64 – 1,920               | 46 – 7,480     | 1.0                      | 1/11                  |
| 0.8                                  | 4.48                         | 910 – 29,300             | 44 – 1,420               | 25 – 4,640     | 1.0                      | 1/21                  |
| 0.9                                  | 5.60                         | 1,060 – 35,800           | 36 – 1,220               | 18 – 3,600     | 1.0                      | 1/29                  |
| 1.0                                  | 6.63                         | 1,200 – 41,700           | 32 – 1,120               | 15 – 3,070     | 1.0                      | 1/37                  |
| 1.1                                  | 7.58                         | 1,340 – 47,200           | 30 – 1,060               | 13 – 2,740     | 1.0                      | 1/45                  |
| 1.2                                  | 8.48                         | 1,460 – 52,400           | 28 – 1,020               | 12 – 2,530     | 1.0                      | 1/52                  |

TABLE A5  
REALIZATION FREQUENCY OF SNE IA ( $\eta_{\text{eff}} = 1$ )

| $M_{\text{WD},0}$<br>( $M_{\odot}$ ) | $\Delta \log A$ | $M_A$<br>( $M_{\odot}$ ) | $M_B$<br>( $M_{\odot}$ ) | $\Delta q$ | $\nu_{\text{WD}}$<br>( $\text{yr}^{-1}$ ) |
|--------------------------------------|-----------------|--------------------------|--------------------------|------------|---|
| 0.8 – 0.9                            | $0.6 \cdot 2/3$ | 4.48                     | 5.60                     | 0.37       | 0.0006                                    |
| 0.9 – 1.0                            | $1.0 \cdot 2/3$ | 5.60                     | 6.63                     | 0.36       | 0.0006                                    |
| 1.0 – 1.1                            | $1.5 \cdot 2/3$ | 6.63                     | 7.58                     | 0.36       | 0.0005                                    |

TABLE A6  
REALIZATION FREQUENCY OF SNE IA ( $\eta_{\text{eff}} = 0.3$ )

| $M_{\text{WD},0}$<br>( $M_{\odot}$ ) | $\Delta \log A$ | $M_A$<br>( $M_{\odot}$ ) | $M_B$<br>( $M_{\odot}$ ) | $\Delta q$ | $\nu_{\text{WD}}$<br>( $\text{yr}^{-1}$ ) |
|--------------------------------------|-----------------|--------------------------|--------------------------|------------|---|
| 0.9 – 1.0                            | $0.7 \cdot 2/3$ | 5.60                     | 6.63                     | 0.21       | 0.0002                                    |
| 1.0 – 1.1                            | $1.1 \cdot 2/3$ | 6.63                     | 7.58                     | 0.23       | 0.0003                                    |
| 1.1 – 1.2                            | $1.8 \cdot 2/3$ | 7.58                     | 8.48                     | 0.23       | 0.0003                                    |





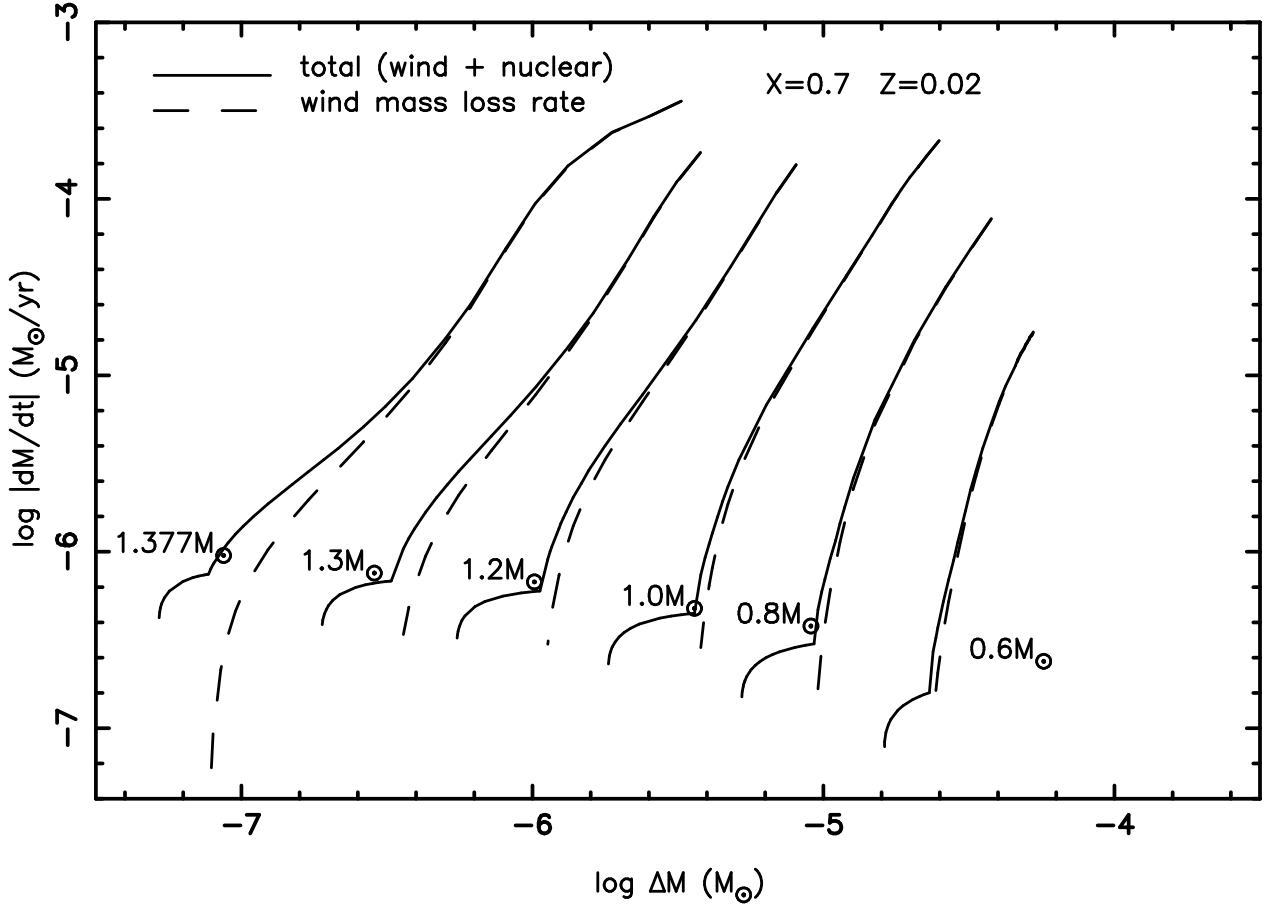


FIG. A2.— Wind mass loss rate  $\dot{M}_{\text{wind}}$  (dashed line) and the total mass decreasing rate of the hydrogen-rich envelope on the white dwarf  $\dot{M}_{\text{nuc}} + \dot{M}_{\text{wind}}$  (solid line), i.e., nuclear burning rate  $\dot{M}_{\text{nuc}}$  plus wind mass loss rate  $\dot{M}_{\text{wind}}$ , are plotted against the envelope mass  $\Delta M$  for WDs with masses of  $0.6M_{\odot}$ ,  $0.8M_{\odot}$ ,  $1.0M_{\odot}$ ,  $1.2M_{\odot}$ ,  $1.3M_{\odot}$ , and  $1.377M_{\odot}$ . White dwarf mass is attached to each line. The metallicity is the solar value of  $Z = Z_{\odot} = 0.02$ . There exists only a static (no wind) solution below the break of each solid line while there exists only a wind solution above the break for a given envelope mass of  $\Delta M$ . The optically thick winds blow when the mass transfer rate from the companion star  $|\dot{M}_2| = |\dot{M}_{\text{nuc}} + \dot{M}_{\text{wind}}|$  exceeds  $\dot{M}_{\text{cr}} = 0.75 \times 10^{-6} (M_{\text{WD}}/M_{\odot} - 0.4) M_{\odot} \text{ yr}^{-1}$ .

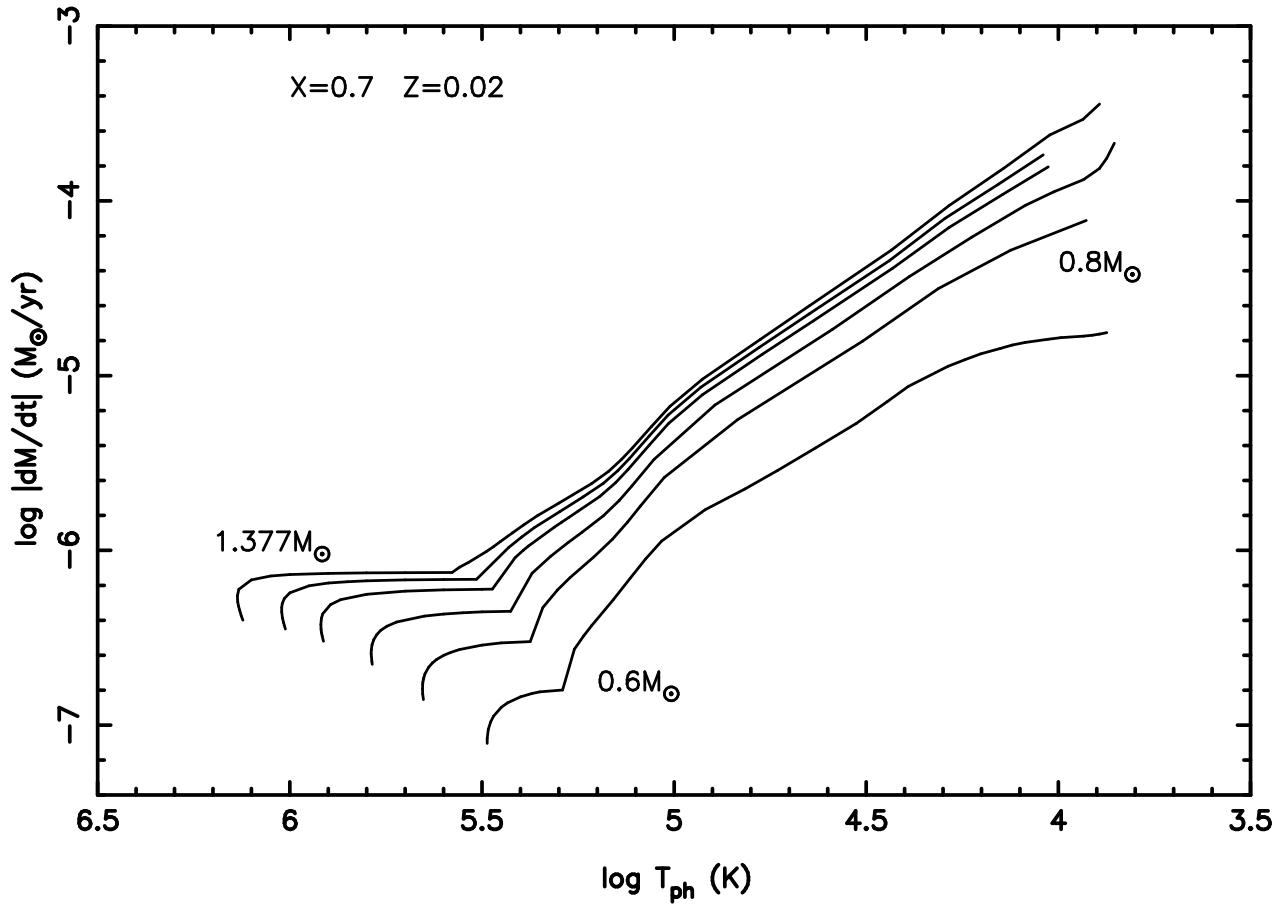


FIG. A3.— Photospheric temperature  $T_{ph}$  is plotted against the decreasing rate of the envelope mass  $\dot{M}_{nuc} + \dot{M}_{wind}$  for WDs with masses of  $0.6M_{\odot}$ ,  $0.8M_{\odot}$ ,  $1.0M_{\odot}$ ,  $1.2M_{\odot}$ ,  $1.3M_{\odot}$ , and  $1.377M_{\odot}$ . Same envelope models as in Fig. 2. Optically thick winds blow when  $\log T_{ph} (K) \lesssim 5.3$ .

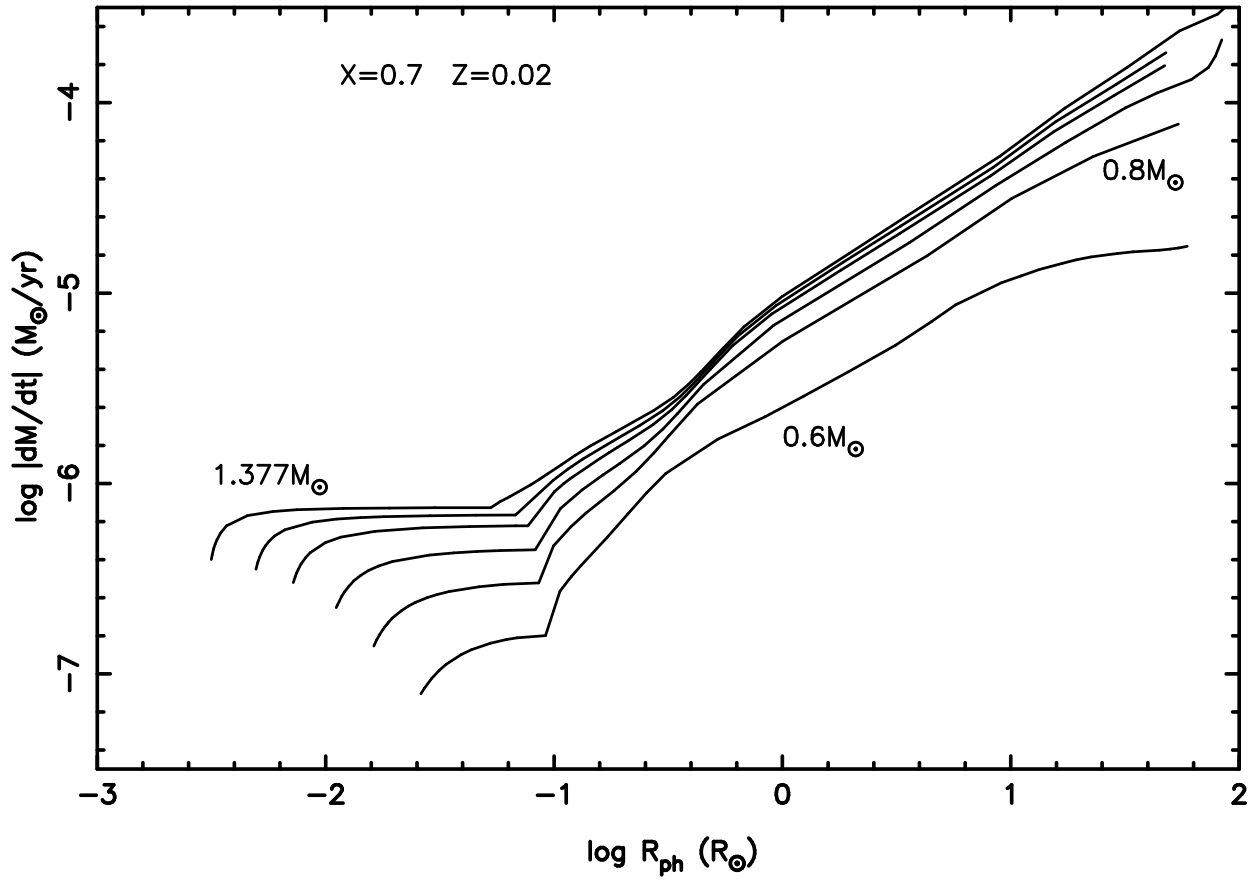


FIG. A4.— Photospheric radius  $R_{\text{ph}}$  is plotted against the decreasing rate of the envelope mass  $\dot{M}_{\text{nuc}} + \dot{M}_{\text{wind}}$  for WDs with masses of  $0.6M_{\odot}$ ,  $0.8M_{\odot}$ ,  $1.0M_{\odot}$ ,  $1.2M_{\odot}$ ,  $1.3M_{\odot}$ , and  $1.377M_{\odot}$ . Same envelope models as in Fig. 2. Optically thick winds blow when  $R_{\text{ph}} \gtrsim 0.1R_{\odot}$ .

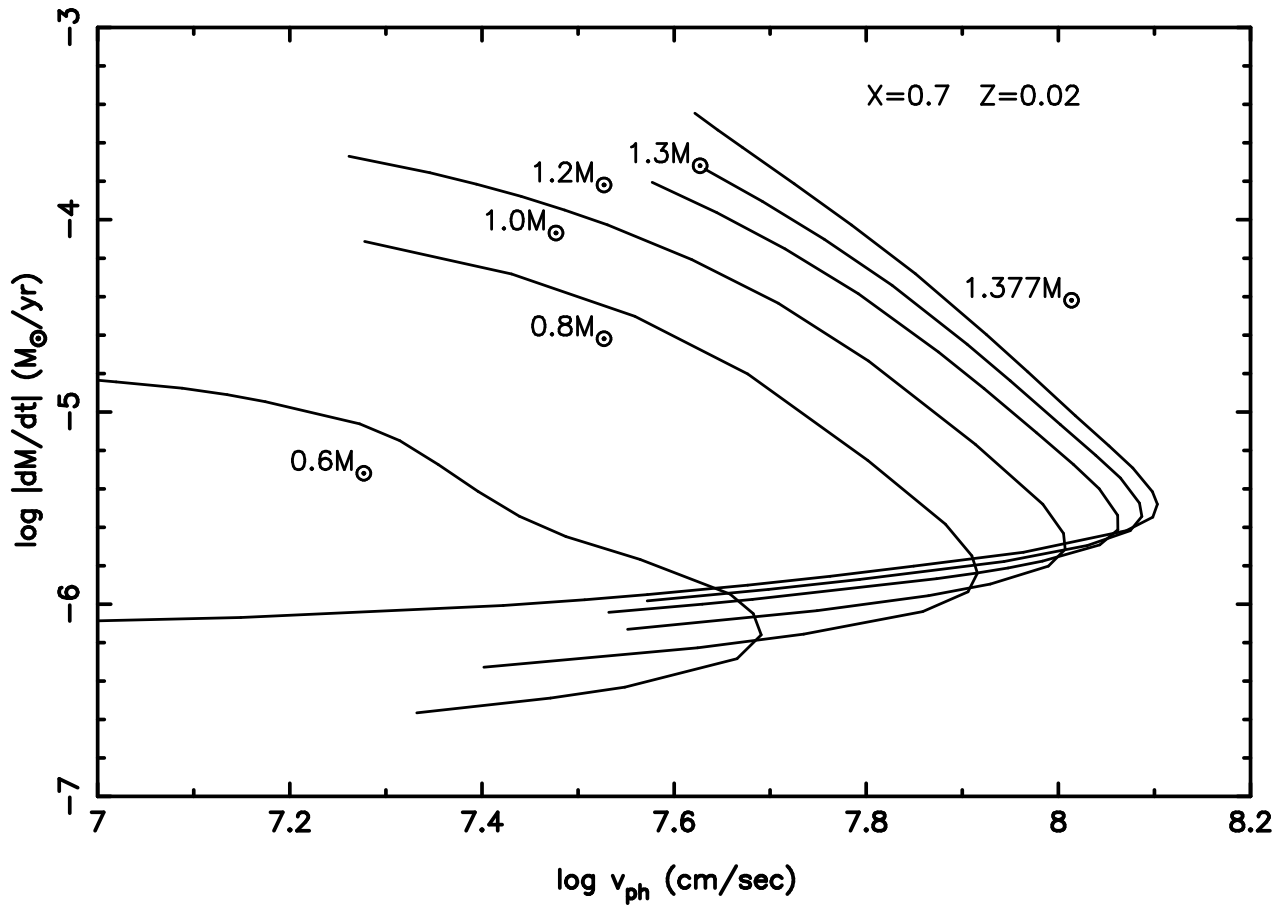


FIG. A5.— Photospheric velocity  $v_{\text{ph}}$  is plotted against the decreasing rate of the envelope mass  $\dot{M}_{\text{nuc}} + \dot{M}_{\text{wind}}$  for WDs with masses of  $0.6M_{\odot}$ ,  $0.8M_{\odot}$ ,  $1.0M_{\odot}$ ,  $1.2M_{\odot}$ ,  $1.3M_{\odot}$ , and  $1.377M_{\odot}$ . Same models as in Fig. 2.

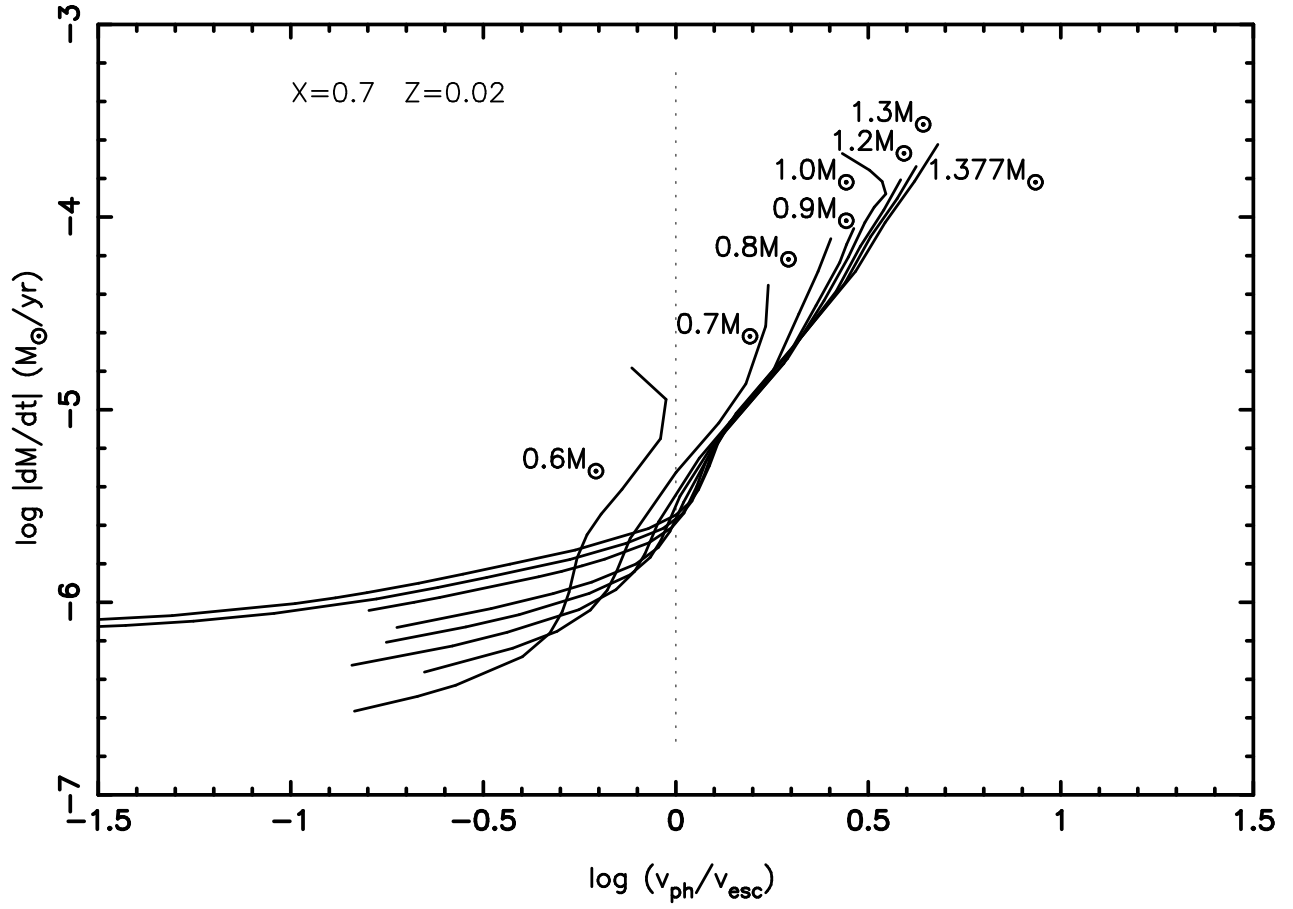


FIG. A6.— Ratio of the photospheric velocity to the escape velocity there  $v_{\text{ph}}/v_{\text{esc}}$  is plotted against the decreasing rate of the envelope mass  $\dot{M}_{\text{nuc}} + \dot{M}_{\text{wind}}$  for WDs with masses of  $0.6M_{\odot}$ ,  $0.7M_{\odot}$ ,  $0.8M_{\odot}$ ,  $0.9M_{\odot}$ ,  $1.0M_{\odot}$ ,  $1.2M_{\odot}$ ,  $1.3M_{\odot}$ , and  $1.377M_{\odot}$ . Same models as in Fig. 2, but  $0.7M_{\odot}$  and  $0.9M_{\odot}$  are added. We regard the wind as “strong” when the photospheric velocity exceeds the escape velocity there, i.e.,  $v_{\text{ph}} > v_{\text{esc}}$ . If not, it is regarded as “weak.”

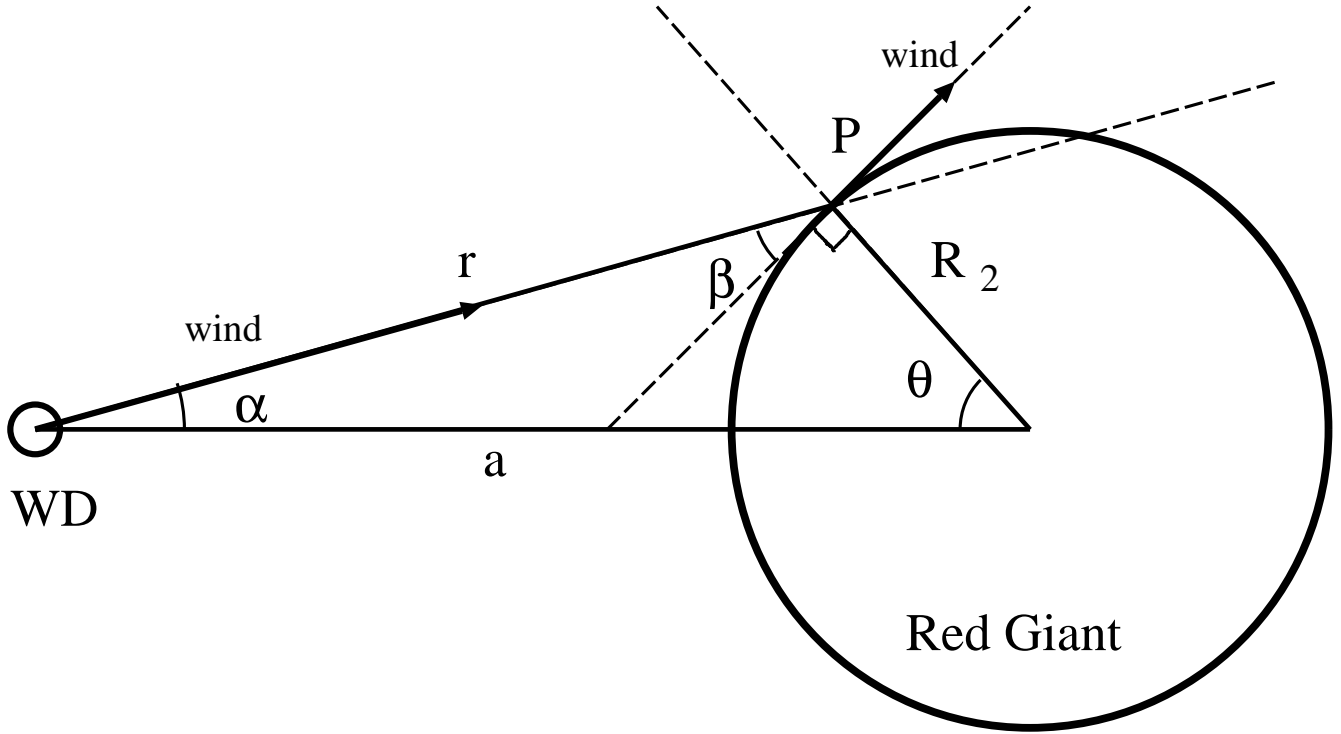


FIG. A7.— Fast winds from the white dwarf (WD) collide with the surface of the red-giant and strip mass from the red-giant. The normal component of the wind velocity to the red-giant surface is dissipated by forming a shock and it heats up the surface. Then, a part of the surface mass is ablated and blown in the wind.

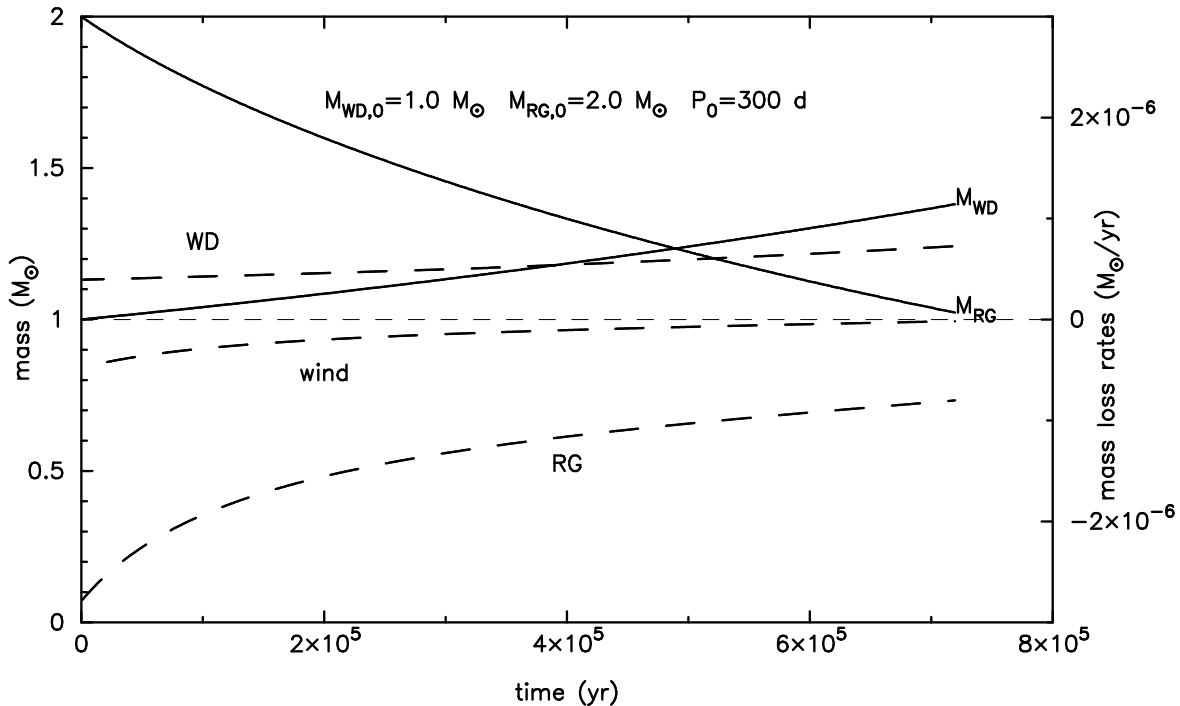


FIG. A8.— Time evolution of an SN Ia progenitor system for case P1 (explosion during the wind phase). The initial parameters are shown at the top of the figure. The white dwarf mass increases to  $1.38M_{\odot}$  and explodes as an SN Ia at  $t = 7.2 \times 10^5$  yr. The solid lines show the masses of the white dwarf ( $M_{\text{WD}}$ ) and the red-giant companion ( $M_{\text{RG}}$ ). The dashed lines show, from top to bottom, the net mass accretion rate onto the white dwarf, the wind mass loss rate, and the mass decreasing rate of the red-giant companion, respectively.

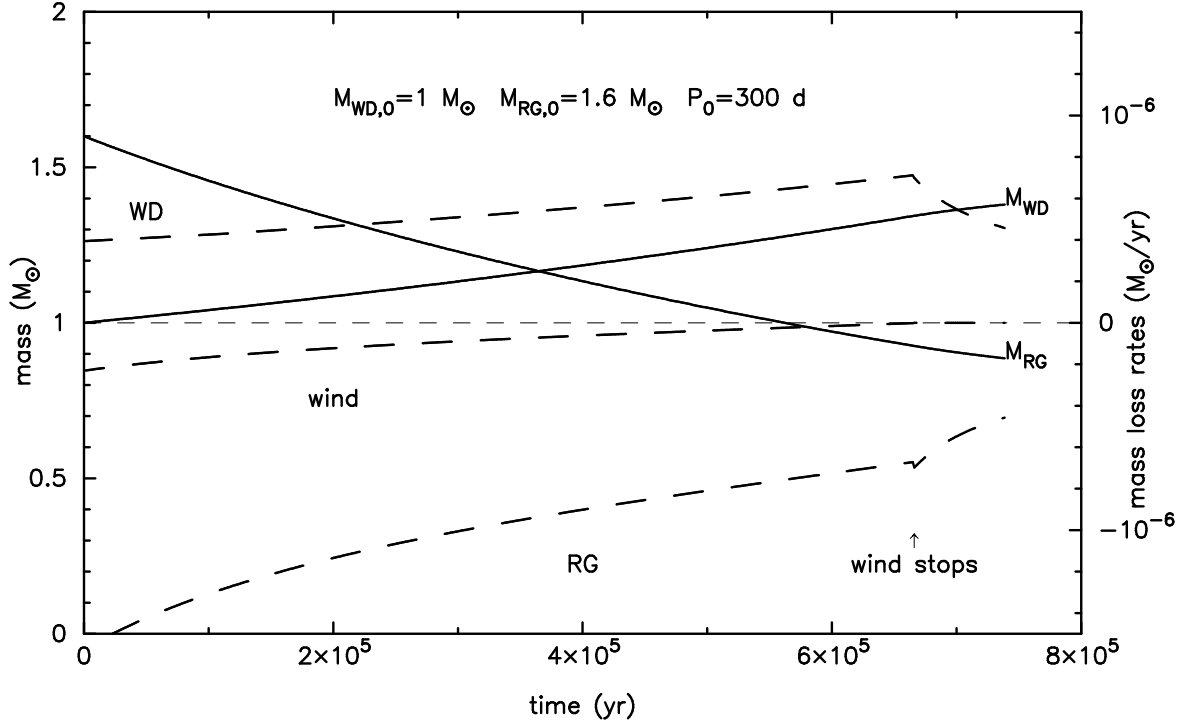


FIG. A9.— Same as Fig. 8 but for case P2 (explosion during the steady hydrogen shell burning phase). The strong wind stops at the time indicated by an arrow. The white dwarf mass increases to  $1.38M_{\odot}$  and explodes as an SN Ia at  $t = 7.4 \times 10^5$  yr.

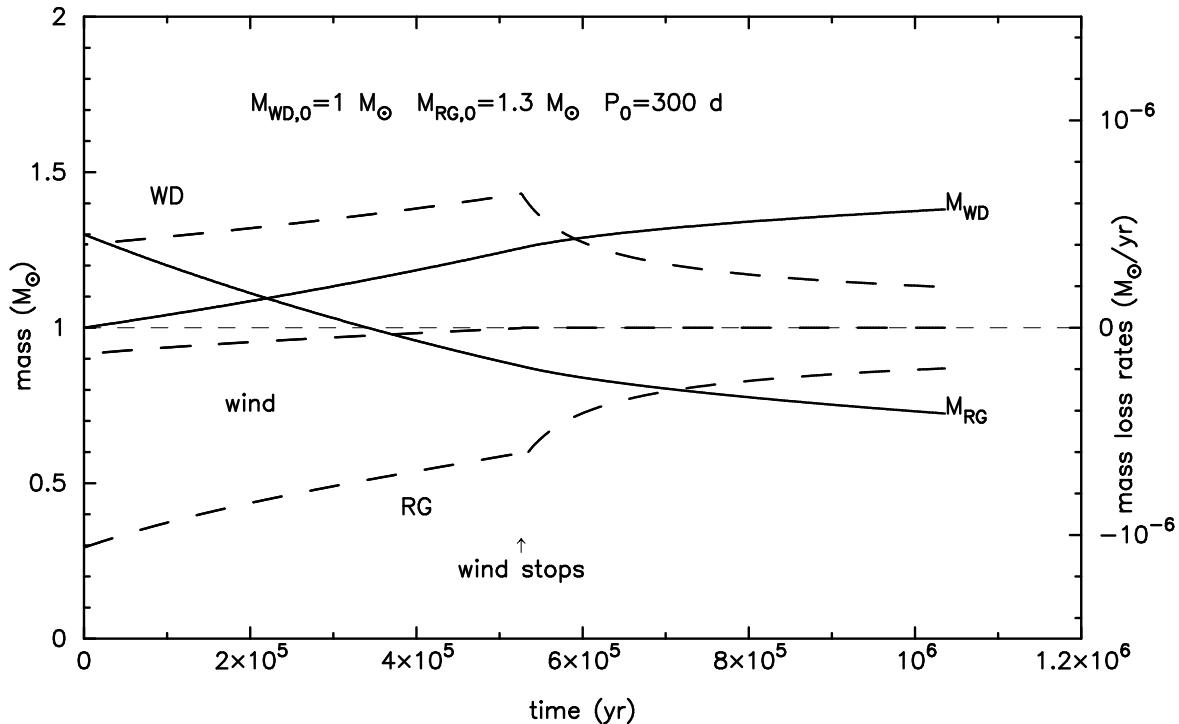


FIG. A10.— Same as Fig. 8 but for case P3 (explosion during the very weak shell flash phase). The strong wind stops at the time indicated by an arrow. The hydrogen shell burning becomes unstable to trigger very weak shell flashes at  $t = 6.5 \times 10^5$  yr. The white dwarf mass increases to  $1.38M_{\odot}$  and explodes as an SN Ia at  $t = 1.04 \times 10^6$  yr.

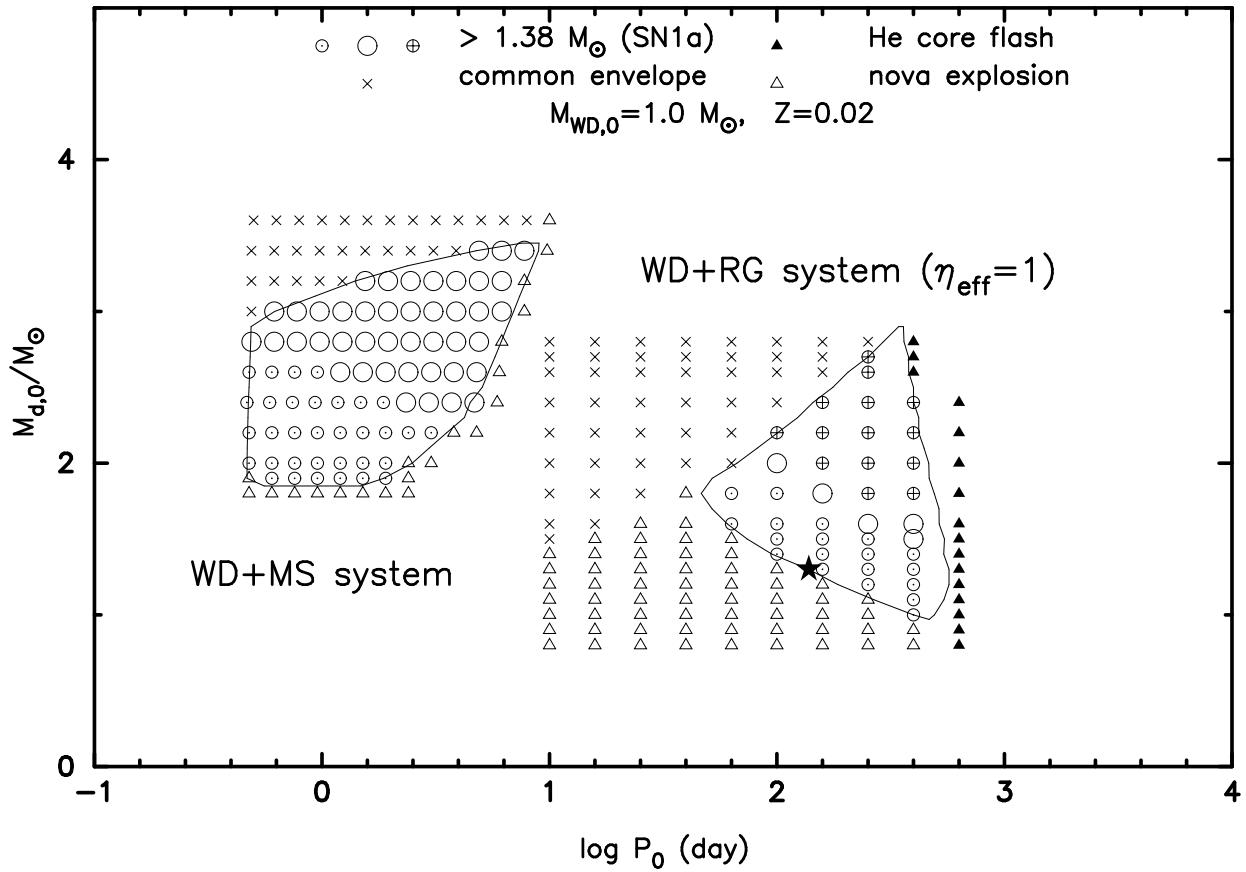


FIG. A11.— Final outcome of close binary evolution in the  $\log P_0 - M_{\text{d},0}$  plane. Here,  $M_{\text{d},0}$  is the donor mass,  $M_{\text{MS},0}$  or  $M_{\text{RG},0}$ . Final outcome is either an unstable mass transfer ( $H_4(q) > 0$ ) at the beginning (forming a common envelope; denoted by  $\times$ ), or an SN Ia explosion (denoted by  $\oplus$ ,  $\circ$ , or  $\ominus$ ) or a nova (denoted by a open triangle), or a central helium flash (denoted by a filled triangle).  $\oplus$ : wind phase at SN Ia explosion (P1).  $\circ$ : wind stops before SN Ia explosion but the mass transfer rate is still high enough to keep steady hydrogen shell burning, i.e.,  $|\dot{M}_t| > \dot{M}_{\text{st}}$  (P2).  $\ominus$ : wind stops before SN Ia explosion and the mass transfer rate is decreasing between  $M_{\text{low}} < |\dot{M}_t| < \dot{M}_{\text{st}}$  at SN Ia explosion (P3). The region producing an SN Ia is bounded by a solid line. The left/right region corresponds to the WD+MS (compact)/WD+RG (wide) system, respectively. A star mark ( $\star$ ) denotes an initial position of T CrB in the WD+RG systems.



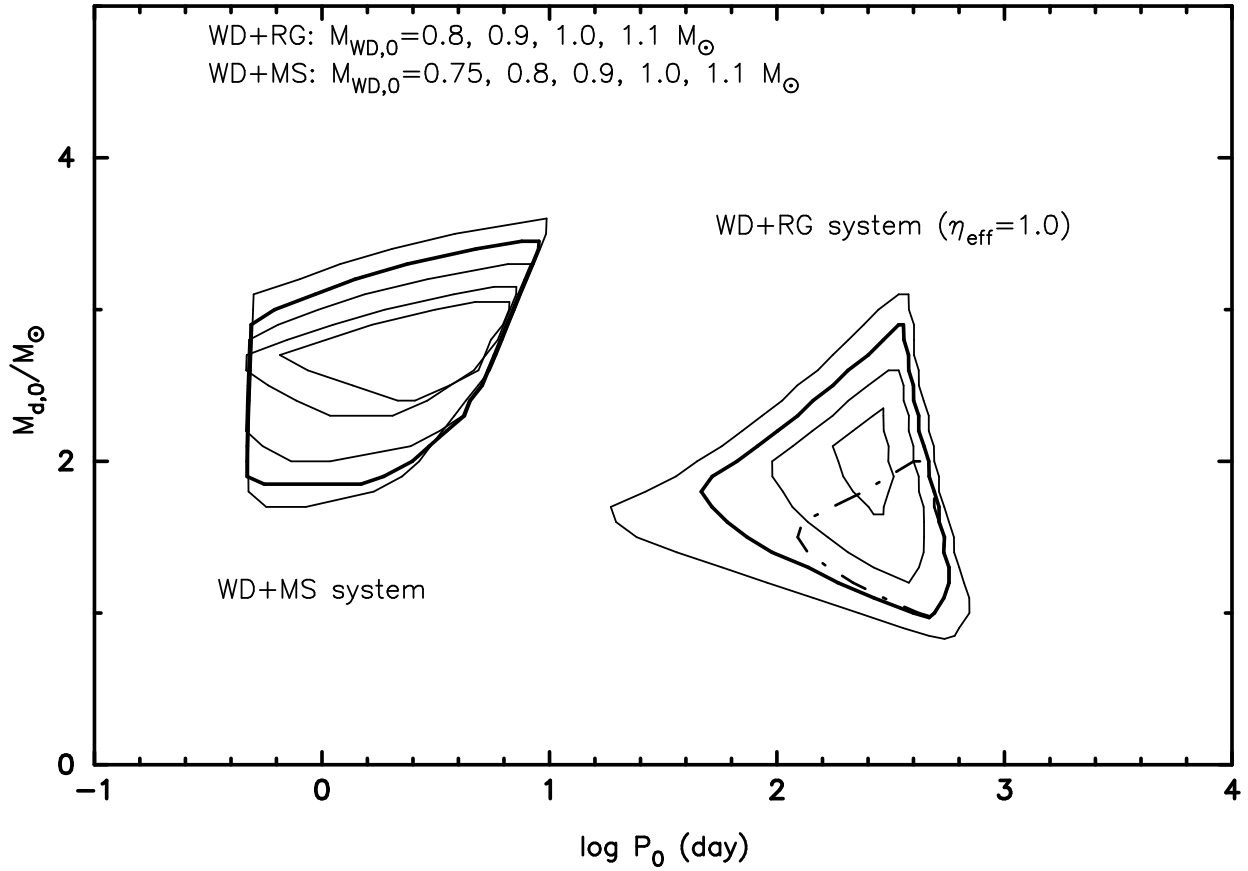


FIG. A12.— The region to produce SNe Ia in the  $\log P_0 - M_{d,0}$  plane for five initial white dwarf masses of  $0.75M_\odot$ ,  $0.8M_\odot$ ,  $0.9M_\odot$ ,  $1.0M_\odot$  (heavy solid line), and  $1.1M_\odot$ . The region of  $M_{WD,0} = 0.75M_\odot$  almost vanishes for both the WD+MS and WD+RG systems, and the region of  $M_{WD,0} = 0.75M_\odot$  vanishes for the WD+RG system. Here, we assume the stripping efficiency of  $\eta_{\text{eff}} = 1$ . For comparison, we show only the region of  $M_{WD,0} = 1.0M_\odot$  for a much lower efficiency of  $\eta_{\text{eff}} = 0.3$  by a dash-dotted line.

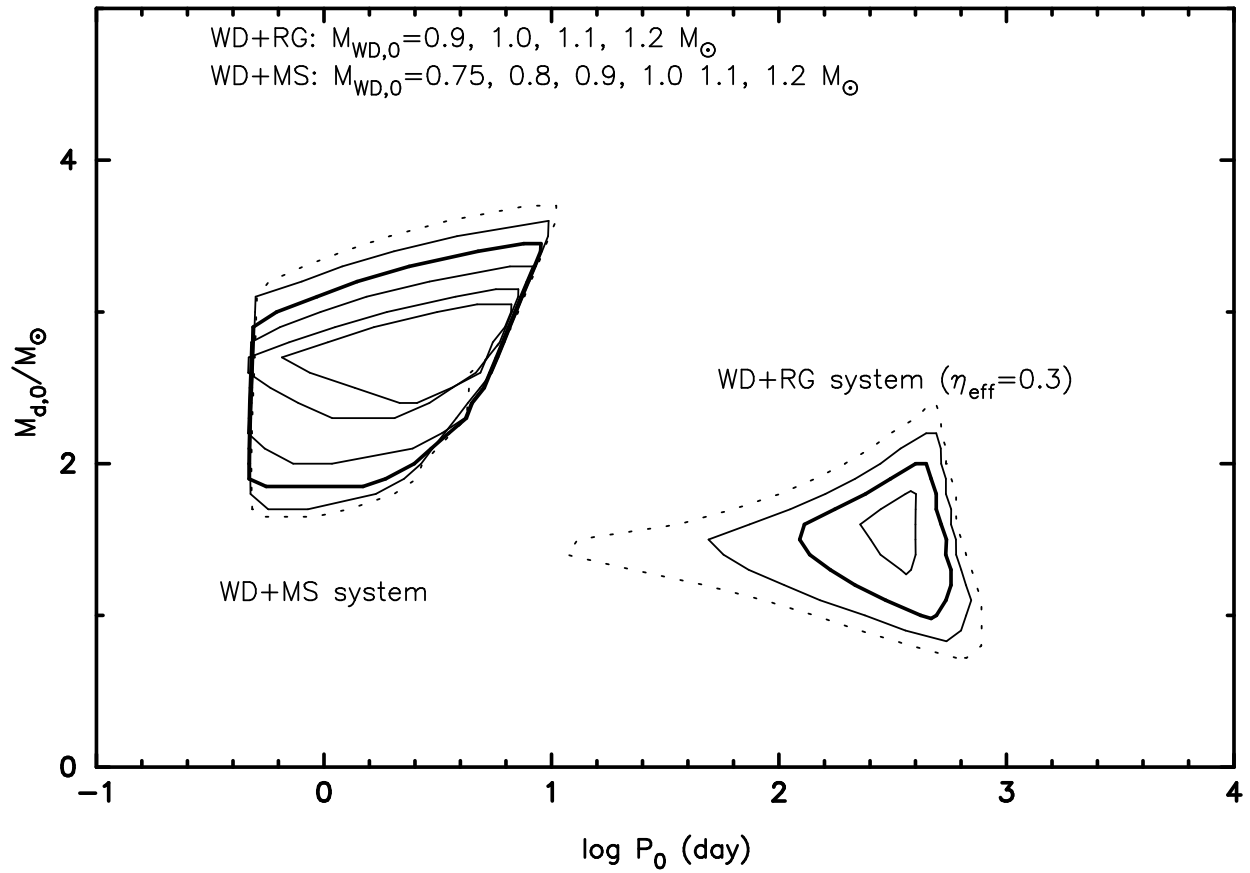


FIG. A13.— Same as Fig. 12 but for the much lower mass-stripping efficiency of  $\eta_{\text{eff}} = 0.3$ . We add the region of  $M_{\text{WD},0} = 1.2 M_{\odot}$  both for the WD+MS/WD+RG systems (dotted lines). The region of  $M_{\text{WD},0} = 0.8 M_{\odot}$  vanishes for the WD+RG system.

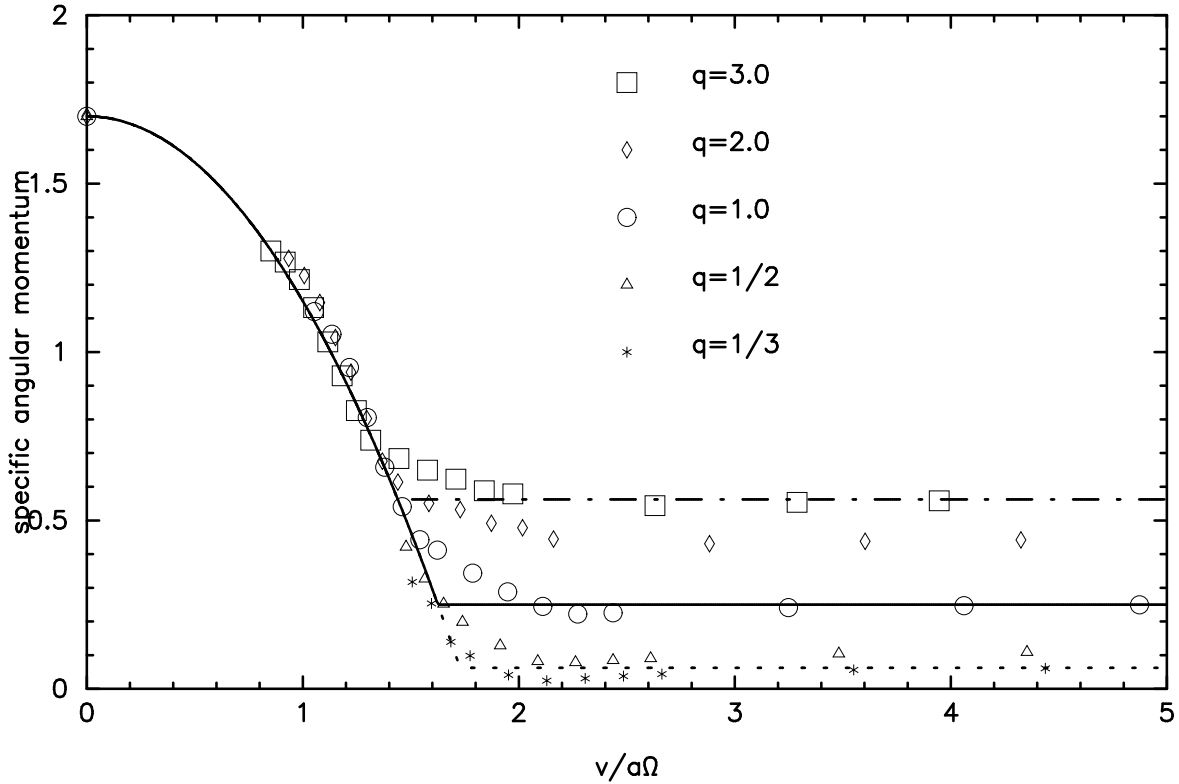


FIG. A14.— Specific angular momentum of wind is plotted against the outflowing velocity near the inner critical Roche lobe. The specific angular momentum and the outflowing velocity are measured in units of  $a^2\Omega$  and  $a\Omega$ , respectively, where  $a$  is the separation and  $\Omega$  is the orbital angular velocity. Five cases of the mass ratio are examined, i.e.,  $q = M_2/M_1 = 3, 2, 1, 1/2,$  and  $1/3$ . It is assumed that the wind blows from the primary. The limiting case of  $\ell_w = 1.7$  for  $v = 0$  is taken from Nariai (1975), Nariai & Sugimoto (1976), and Sawada et al. (1984).